

# Universität Bonn

## Institut für Angewandte Physik

### **Quantum Register Initialization via Deterministic Atom Sorting in Optical Lattices**

Deena Kim

Institut für Angewandte Physik  
Universität Bonn  
Wegelstr. 8  
D-53115 Bonn



BONN-IR-2012-XXX  
September 2012



# Universität Bonn

## Institut für Angewandte Physik

### **Quantum Register Initialization via Deterministic Atom Sorting in Optical Lattices**

Deena Kim

Dieser Forschungsbericht wurde als Masterarbeit von der Mathematisch-Naturwissenschaftlichen Fakultät der Universität Bonn angenommen.

Angenommen am: 28.08.2012  
Referent: Prof. Dr. Dieter Meschede  
Koreferent: Prof. Dr. Stefan Linden



# Contents

<b>1</b>	<b>Introduction</b>	<b>1</b>
<b>2</b>	<b>State-Dependent Transport in a 1D Optical Lattice</b>	<b>3</b>
2.1	Experimental Setup . . . . .	3
2.2	Continuous Transport of Atoms in One Direction . . . . .	7
2.3	Transport Efficiency . . . . .	7
<b>3</b>	<b>Deterministic Atom Sorting</b>	<b>11</b>
3.1	Error Correction Through Feedback . . . . .	11
3.2	One Atom Movement to Target Position . . . . .	13
3.2.1	Feedback Conditions . . . . .	13
3.2.2	One Atom Results . . . . .	14
3.3	Bringing Two Atoms Together to Target Separation . . . . .	21
3.3.1	Magnetic Field Gradient Calibration . . . . .	21
3.3.2	Adiabatic Passages . . . . .	21
3.3.3	Feedback Conditions . . . . .	28
3.3.4	Determination of Maximum Steps . . . . .	29
3.3.5	Two Atom Results . . . . .	31
<b>4</b>	<b>Conclusion</b>	<b>37</b>
<b>5</b>	<b>Next Steps and Prospects for Continuing Work</b>	<b>39</b>
	<b>Bibliography</b>	<b>41</b>
	<b>Acknowledgements</b>	<b>43</b>



# Chapter 1

## Introduction

There has been much interest since the first formulation of quantum mechanics in the 1920's to perform experiments testing new theories. Since then, the field has expanded immeasurably and has become a fundamental groundwork for understanding all other aspects of physics. However, gaining a better understanding behind fundamental quantum processes through computer modeling has been limited due to the classical nature of computers. Then in the 1980's, during the peak of computer miniaturization, came the quantum computer which exploited the smallness of atoms, ions, and photons and embedded information in their discrete states [1]. A quantum computer is the quantum analog to the standard, classical computer but which operates on data stored in the form of qubits (quantum-bits). The essential difference between classical and quantum data stems from the fact that a quantum state can be represented by either pure qubits  $|0\rangle$  or  $|1\rangle$ , or a mixed superposition of qubits, whereas a classical state can only be represented by either bits 0 or 1 and not both at the same time. This factor for larger storage capability gives quantum computers certain advantages over classical ones, especially regarding its computing capacity for simulating quantum systems. For example, to simulate an  $n$ -qubit system, a classical computer would have to store  $2^n$  complex values [2]. Its computational time is exponential, whereas for a quantum computer, the time is polynomial. The field of quantum information has grown in popularity ever since, with a plethora of different setups for demonstrating a quantum computer.

One such setup are neutral atoms trapped in optical lattices. Not only do the neutral atoms avoid interactions with the outside environment, unlike ions, another popular tool for realizing a quantum computer, but they are also well localized and separated from each other. They also have stable energy states, allowing for selective and individual manipulation. In this setup as well as in many others, the use of a two-level energy scheme of neutral cesium (Cs) atoms allows for the selection of the hyperfine levels of the ground state as qubit representations. Already, state-dependent transport has been used within our one-dimensional (1D) optical lattice to implement single-atom interferometers [3] as well as to demonstrate quantum walks (the analog to classical walks) in position space [4].

While our overall motivation is to use state-dependent transport to demonstrate the following concepts of quantum information theory, the specific interest of my Masters project and the content of this thesis is rather the preparation of predefined patterns of individual atoms for applications as quantum registers. A quantum register, which has a well-defined number of qubits, is required in most conventional forms of quantum computational processing. The register must be able to store information encoded into its memory and then later process this information, via means of quantum logic gates [2]. Quantum register initialization can already be established if we manage to sort the atoms by their qubit states within the optical lattice into any arbitrary pattern. Another interesting application for atom sorting is to bring two atoms together into a single lattice site for coherent collisions, where atom-atom interactions lead to quantum correlated states, including entangled states.

To successfully implement this requires several steps combining our present state-dependent transport, individual atom addressing, and feedback methods for error correction. The basic logic behind our feedback can be seen in Fig. 1.1. We repeat the feedback loop of transporting atoms and each time,

take an image to see where the atoms have moved until they have reached the target orientation. With this basic scheme, we perform experiments first to transport a single atom to an absolute position on the optical lattice, and then increase the complexity by bringing two atoms together to a predetermined separation. It should be noted that these experiments utilize classical transport because we sort atoms of pure qubit states and not wavepackets of superposition states as is done for quantum walks [4]. Quantum atom sorting would require us to shorten the feedback operations from a ms to  $\mu$ s timescale to operate within the decoherence time of cesium.

The methods and results of these experiments are presented in this paper, following an introductory overview of our well-established state-dependent transport.

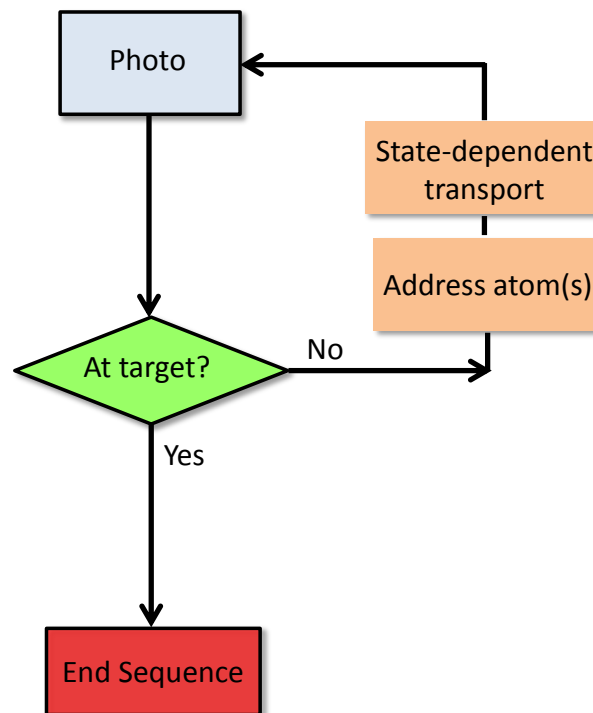


Figure 1.1: Atom sorting feedback scheme: A photo gives us information of where the atoms are so that we can check if transport succeeded and then end the sequence. If the atoms are not at target, we repeat the loop consisting of addressing the atom and then applying state-dependent transport.

## Chapter 2

# State-Dependent Transport in a 1D Optical Lattice

### 2.1 Experimental Setup

Neutral Cs atoms are first collected and cooled from background gas into a three-dimensional (3D) magneto-optical trap (MOT). At this point, we form a 1D optical lattice by superposing two counter-propagating, linearly polarized beams of far-detuned light with a wavelength of  $\lambda_{\text{lattice}} = 866$  nm. A basic scheme of our experimental setup can be seen in Fig. 2.1. The overlap of the beams gives rise to a standing wave dipole trap. This attractive periodic potential traps atoms inside its wells, as seen in the magnification inset of the figure. The wells, otherwise referred to as lattice sites, have both a spacing and periodicity of  $\lambda_{\text{lattice}}/2 = 433$  nm within a span of  $100 \mu\text{m}$  in the measurement region: corresponding to a total of around 200 lattice sites [5].

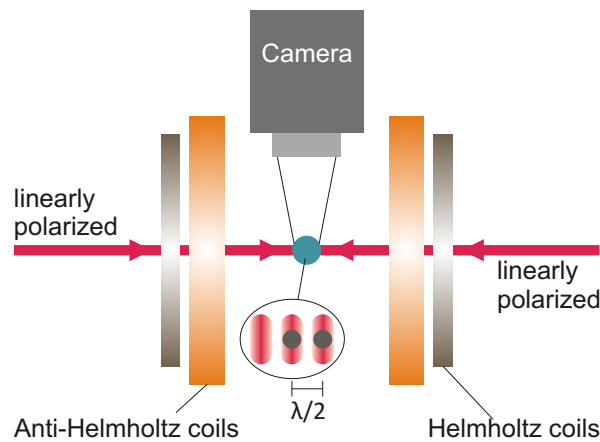


Figure 2.1: Experimental Setup [5]: Counter-propagating beams overlap to form the 1D optical lattice. A zoom inset shows atoms trapped within the wells of the dipole trap, spaced apart by  $\lambda_{\text{lattice}}/2 = 433$  nm. The camera detects atom fluorescence for imaging and the Helmholtz/anti-Helmholtz coils are used to create a constant magnetic field/magnetic field gradient. The weak field from the Helmholtz configuration is responsible for the energy level degeneracy in Fig. 2.2

The camera, consisting of a microscope objective and an electron-multiplying (EM) CCD chip sensor, is placed over the lattice where the atom fluorescence is captured and then imaged onto the chip for up to 1 s.

Surrounding the lattice area are Helmholtz and anti-Helmholtz coils which are configured to produce a weak magnetic guiding field and a magnetic field gradient, respectively. The guiding field is responsible for the Zeeman splitting of the hyperfine energy levels to which we choose our qubit states in Fig. 2.2. The quadrupole field is used to spatially resolve the individual atoms, addressing them for multiple-atom transport applications, to be described in Sec. 3.3.1.

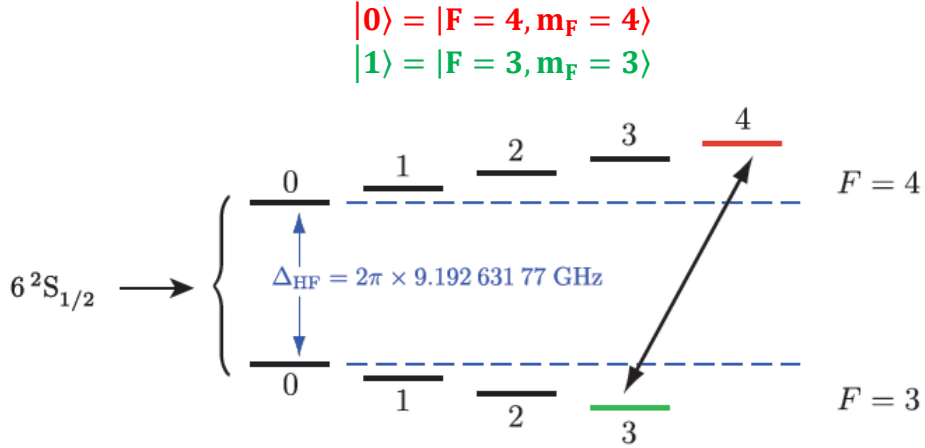


Figure 2.2: Selection of qubits from the Zeeman levels of Cs ground state [6]: The energy difference of the hyperfine levels of  $F = 3$  and  $F = 4$  (blue dashed lines) corresponds to 9.2 GHz frequency. The additional Zeeman splittings away from the central hyperfine levels (indicated by  $m_F$  integers all of which are not displayed in this figure) arise due to the weak magnetic field. Our chosen qubit states are the outermost Zeeman states of  $|F = 4, m_F = 4\rangle$  and  $|F = 3, m_F = 3\rangle$ .

Arising from the electronic ground state of Cs ( $6^2S_{1/2}$ ) are the hyperfine states,  $F = 3$  and  $F = 4$ , spaced apart by  $\Delta_{\text{HF}}$  (Fig. 2.2). Further non-degenerate Zeeman levels arise out of the two hyperfine levels due to the presence of the weak magnetic field (strength of 3 G) with a level separation scaling linearly with the magnetic field strength. We use the outermost Zeeman levels as our two qubits since the transition can be tuned quite far from any other possible transitions and for reasons of reliable population transfer between the two states. The ability to control and ascertain information about the atom's state is crucial to the success of the experiment. Most importantly however, higher values of  $m_F$  have stronger polarization selectivity than lower values. It is this selectivity which is needed for state-dependent transport.

For qubit sorting, we need to be able to transport our atoms along the lattice in a way that is specific to their states. And this can be done by taking advantage of the selectivity of our beam's polarization components. Fig. 2.3 shows the fine structure energy levels of Cs indicated by quantum spin numbers  $m_J$  and  $m_J$ . Since we are looking at the spin-coupling, we can neglect the hyperfine structure since its energy level spacing is orders of magnitude smaller than for the fine structure splittings. The upper, blue dashed line between the excited states represents the frequency that our lattice beams are tuned to with an energy per photon of  $\hbar\omega$ . For both of the qubits in the ground state, the linearly polarized lattice beam can be decomposed into its circular polarization components  $\sigma^+$  and  $\sigma^-$  as shown by the red and green transition arrows. The excited spin states within  $6^2P_{3/2}$  and  $6^2P_{1/2}$ , are the allowed possible transition states according to the selection rule of  $\Delta m_J = \pm 1$  for  $\sigma^\pm$ . We choose our light field to be blue-detuned to

the  $6^2P_{1/2}$  transition (creating a repulsive potential) and red-detuned to the  $6^2P_{3/2}$  transition (attractive potential). This in effect cancels the inner, fine structure components ( $m'_J = \pm 1/2$ ) while leaving the outer, attractive potential transitions. We are thus able to trap atoms in a specific potential according to their states and perform for state-dependent transport. The  $|0\rangle$  qubit (or spin up) is trapped by the minima of a  $U_{\sigma^+}$  potential, and the  $|1\rangle$  qubit (spin down) by the  $U_{\sigma^-}$  potential [7].

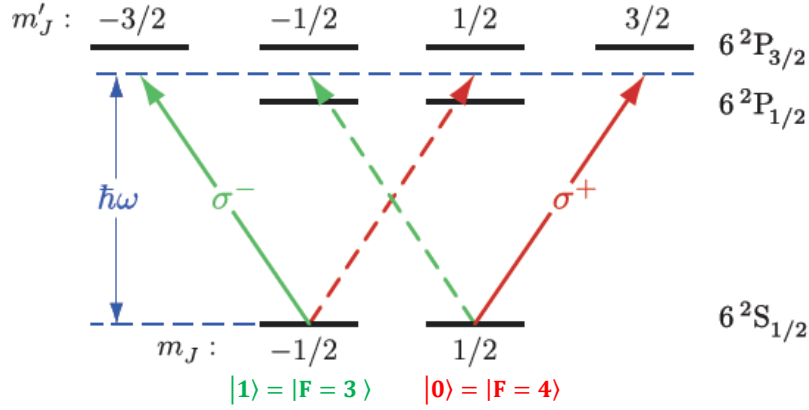


Figure 2.3: State-selective potentials created by  $\sigma^\pm$  circular polarization components of the light field [6]: The qubit states are represented by the fine structure levels  $m_J = \pm 1/2$  (spin up and spin down). The linearly polarized light which is decomposed into its circularly polarized components, is detuned between the upper excited states, creating attractive and repulsive potentials. The inner transitions' ( $m'_J = \pm 1/2$  of the  $6^2P_{1/2}$  and  $6^2P_{3/2}$  levels) cancel each other out, leaving just the outer attractive potentials. Thus,  $|1\rangle$  and  $|0\rangle$  both feel different potential components.

We exploit the specific response of the atom's spin states and employ the following scheme to separate the potentials in space, as seen in Fig. 2.4. In the figure,  $\theta$  represents the tilt angle between the polarizations of the counterpropagating beams forming the optical lattice. At first the lattice is fully linearly polarized and then as  $\theta$  rotates,  $U_{\sigma^+}$  and  $U_{\sigma^-}$  shift spatially in opposite directions relative to each other. Meanwhile, the atoms of different spins, move along with their corresponding potentials until the components fully overlap again at  $\theta = \pi$ . Thus, for a rotation of  $\theta = \pi$ , a single atom moves by half a lattice site distance relative to its initial position and for  $\theta = n\pi$  the potentials fully overlap in space.

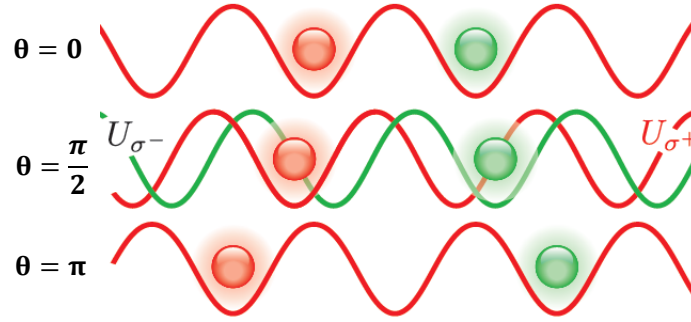


Figure 2.4: Transporting atoms by shifting state-selective potentials [6]: When the angle between polarizations  $\theta$ , is zero, the potentials are overlapped. As  $\theta$  increases, the potential components shift apart, transporting their trapped states with them until overlapping again at  $\theta = \pi$  and each atom is displaced by half of a lattice site distance from its starting position.

We rotate the tilt angle  $\theta$  using an electro-optical modulator (EOM). Fig. 2.5 illustrates how the EOM is used in our setup. The source beam is split into two arms and sent to the target region of the Cs atoms from opposite directions to overlap and form the optical lattice. While both beams are initially vertically polarized, one of the counter propagating arms, Arm 2, passes through the EOM where its polarization acquires a phase shift between its orthogonal components along the orientation of the EOM's principle axes. The phase shift is induced by voltage application to the EOM through a voltage amplifier and is directly proportional to the magnitude of voltage applied. A quarter wave-plate ( $\lambda/4$  plate) further acts to rotate the polarization vector by  $45^\circ$ , leading to a tilt angle of  $\theta = \pi V/V_{\lambda/2}$ , where  $V_{\lambda/2} = 750$  V is the half-wave voltage for  $\lambda = 866$  nm. We see that the extent of  $\theta$ -rotation depends on the half-wave voltage which is also dependent on the wavelength of the crossing beams. However, the tilt angle is finite and limited by  $V_{\max} = 750$  V which the voltage amplifier can deliver thereby leaving up to a maximum rotation of  $\theta_{\max} = \pi$  [7]. Due to the instrumental limitations that restrict us from being able to continuously transport in one direction by infinitely increasing  $\theta$ , we utilize an alternative method described in the next section, that involves shifting  $U_{\sigma\pm}$  back and forth with the EOM meanwhile flipping the atom between spin states by microwave (MW) pulses tuned at the  $|0\rangle \rightarrow |1\rangle$  transition.

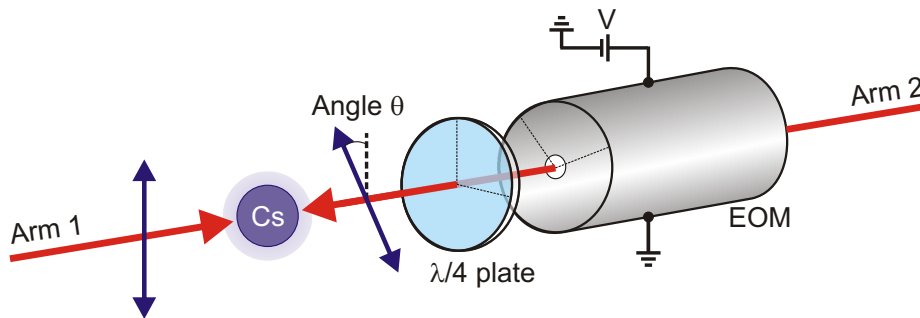


Figure 2.5: Variation of the tilt angle  $\theta$  by use of an EOM: Two counter propagating arms, originating from the same beam with vertical polarization, overlap in the trapping region where the Cs atoms are located. Arm 2 passes through an EOM and a  $\lambda/4$  plate where its polarization is rotated by  $\theta$  relative to its entrance polarization.  $\theta$  is proportional to the voltage applied to the EOM. (Adapted from [6])

## 2.2 Continuous Transport of Atoms in One Direction

To continuously transport an atom in a single direction over several lattice sites, we utilize a transport sequence which does not require going beyond  $\theta_{\max}$  (see Fig.2.6). The sequence consists of an initial image followed by state initialization where we simply prepare the atoms into the spin up state ( $|0\rangle$ ) through optical pumping. The main operations consist of double transport steps, where a single transport step is defined as an EOM shift and one MW  $\pi$ -pulse combination. An EOM shift refers to the relative displacement of the  $U_{\sigma\pm}$  potentials as a result of a voltage ramp to the EOM, as previously described in Sec. 2.1. The double transport step sequence can be seen in further detail in Fig. 2.6b and Fig. 2.6c. For voltages of  $V = 0$  and  $V = V_{\lambda/2}$ , the potentials are fully overlapped in space and it is during this constant voltage where we perform additional operations such as applying a MW pulse to flip the state, or fluorescence imaging. A MW pulse is essential for this sequence as it flips the atom's state before each voltage ramp reversal. When the direction of the ramp is reversed to ramp down,  $U_{\sigma+}$  and  $U_{\sigma-}$  will shift apart but in opposite directions compared to the shift directions during a ramp up. Flipping the state of the atom ensures that it will continue moving in the same direction by alternating between trapping potentials. Otherwise, with no MW pulse, the atom moves back and forth with its corresponding trapping potential along the lattice. Finally, one should keep in mind that the EOM should have zero voltage before imaging because it cannot maintain stability under high voltages for more than 100 ms at a time (our imaging time is  $\sim 1$  s). This implies that only an even number of transport steps are possible between imaging in order to return the EOM to its zero voltage state.

State-dependent transport has been successfully demonstrated using our setup as well as this EOM and MW pulse, combination scheme. However, it has been limited to a distance of several lattice sites [7]. Even with periodic optimization of lab conditions through beam and optical components alignment, transport efficiency decreases exponentially over long distances due to an accumulation of small errors.

## 2.3 Transport Efficiency

The main contributor limiting transport comes from the MW pulse used for flipping the spin-states of the atoms from their initial,  $|0\rangle$  ( $F = 4$ ) state, to  $|1\rangle$  ( $F = 3$ ). We use a rectangular MW  $\pi$ -pulse of  $10 \mu\text{s}$  with a frequency centered at 159.81 MHz. The 159.81 MHz, produced by a vector signal generator, is mixed onto a 9.04 GHz carrier from a fixed frequency source to output the required resonance frequency of 9.2 GHz. To get the ratio of population transfer to the  $F = 3$  state as well as to determine the position of exact resonance frequency, we apply a series of MW pulses of varying frequencies within the range of 159.73–159.93 MHz and measure the percentage of atoms remaining in the lattice after push-out. Push-out is a procedure that uses the radiation pressure force of a beam tuned to the  $F = 4 \rightarrow F = 5$  transition to literally push the  $F = 4$  state atoms out of the trapping potential [7]. The result of such measurements has a sinc-shaped spectrum with a narrow bandwidth and high population transfer probability. Fig. 2.7 is an example spectrum taken from experiment. The spectrum shows a 99% population transfer into the  $F = 3$  state centered at 159.81 MHz, indicating a 1% inefficiency due to the push-out.

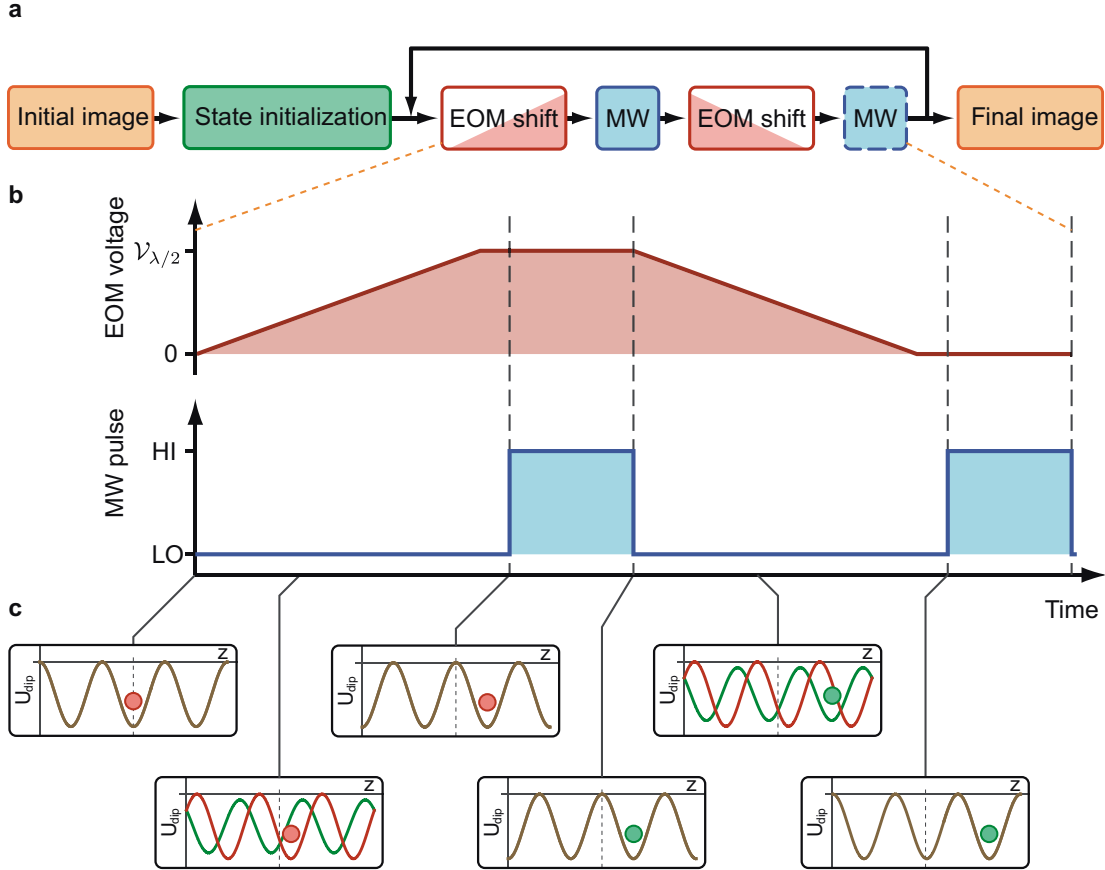


Figure 2.6: Typical transport sequence which occurs between an initial and final image [7]: (a) Sequence operations consist of state initialization, followed by a double-step transport before final imaging. The last MW pulse is required only if we perform another loop. (b) This inset of the double-step transport operations shows the voltage signals sent to the EOM and MW generator. (following the plots from left to right in time). The first EOM shift consists of a voltage ramp up to  $V_{\lambda/2}$  and is held there during the short duration of a MW pulse. The voltage is ramped back down to zero followed by another MW pulse before a final image is taken. (c) Pictorial representation of an atom transported along the  $z$ -axis (lattice axis): At the start when there is no EOM voltage, the potential components are fully overlapped as indicated by the single, brown lattice. During an up ramp of the voltage however, the  $U_{\sigma\pm}$  potentials (indicated by red and green lattices) separate in space. The potentials move their corresponding trapped atom (indicated also red or green) along with them until they overlap again when the EOM voltage equals  $V_{\lambda/2}$ . The spin of the atom is flipped so that during the down ramp voltage, when the  $U_{\sigma\pm}$  separation direction is reversed, the trapped atom can continue moving along the same direction.

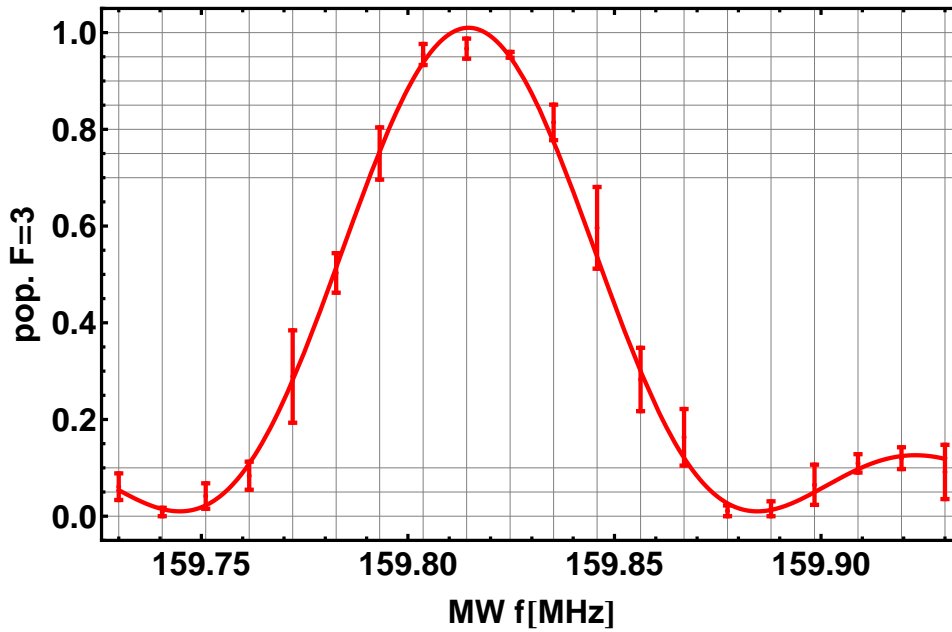


Figure 2.7: MW pulse population transfer spectrum: The percentage of atoms in the  $F = 3$  state vs. frequency. The spectrum exhibits a sinc shape and yields 99% efficiency at the center frequency of 159.81 MHz (mixed onto a fixed frequency to produce the required 9.2 GHz transition frequency). Outside the peak, the efficiency drops quickly and oscillates at the edges.

Despite the high operation efficiency of the MW pulse, transporting over many lattice sites becomes very difficult due to an accumulation of the error with each transport step. Propagation of a finite probability  $P < 1$ , over  $n$  steps goes as  $P^n$  and decays exponentially as seen in Fig. 2.8. The data is taken by loading a group of atoms, transporting all of them by a number of steps and then measuring the actual percentage of atoms which moved by the correct amount of lattice sites. Here with such a high probability of  $P = 99\%$  per transport step, one can already see that the success of transport drops to below 60% after 40 steps. A practical solution for successfully transporting atoms is to split the transport into a series of fewer steps, following by imaging. Thus, we can monitor if transport errors occur by looking at the images and thereby correct the error in the next movement.

Although they do not contribute directly to the transport efficiency, atom losses are still a main factor for transport. The losses occur from background gas collisions which supply the atoms with enough kinetic energy to escape from the lattice site. The  $1/e$  lifetime due to background collisions is roughly 30 s. Losses can also result from improper state initialization or unsuccessful state conversion, which would mean that the atoms escape from their corresponding potential traps during transport. Furthermore, losses occur during imaging due to lowering the dipole trap and temperature in the imaging molasses, producing a rate of 3% atom loss per shot. Since we want to minimize the losses during transport it follows to use a balance between the least number of photos as well as the most number of transport steps to transport an atom successfully.

The subject of the next chapter as well as the focus of my Masters project is on the application of our feedback scheme where I will present the results of several successful experiments that overcome the transport efficiency limitation and transport atoms over longer distances to predetermined positions.

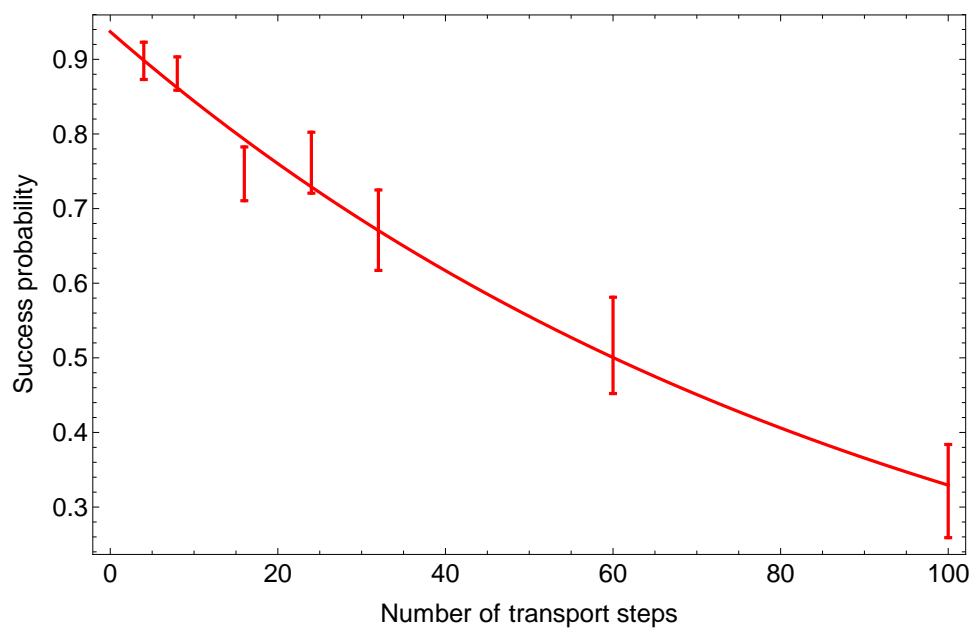


Figure 2.8: Probability of transport success for  $P = 99\%$  per step: The probability for successful transport reduces exponentially as we increase the number of transport steps to move the atom by, even with such a high initial probability. This is why feedback is needed to transport an atom over longer distances and to correct faulty movements.

# Chapter 3

## Deterministic Atom Sorting

### 3.1 Error Correction Through Feedback

Atom sorting and transport can be achieved with the help of real-time feedback for fixing errors and adjusting variable parameters during the transport sequence. The determination for how to react is based on information from the atom images. The basic feedback scheme can be seen in Fig. 3.1. We start by executing a sequence that consists of operations for preparing the experiment, such as loading the MOT, or loading the atoms, just to name a few. Then the camera takes the first image and assuming that we want to continue the sequence with this atom loading (if no atoms are loaded or too many atoms are loaded so that the camera software cannot resolve individual positions, we immediately discard the set and end the sequence), we go on to state initialization via optical pumping of the atoms to the  $|0\rangle$  state. We then follow with a reaction procedure that is dependent on what we see in the image. For example, a reaction can consist of a given number of transport steps to move atoms to a destination position. The only requirement is that the reaction together with optical pumping must be shorter than the  $T_1$  longitudinal relaxation time (measured for our Cs atoms to be 200 ms), which describes the population decay into a steady state. This ensures that operations are done on a definite and known, spin up or spin down state. Following the reaction is another image which tells us whether the reaction was successful or if we should continue reacting. If the end result is achieved, we can proceed to the end of the sequence. If we want to react again however, we enter into another reaction loop and repeat the procedure until we are satisfied with the final image. Therefore, a single sequence or run can consist of a number of reactions depending on how many times we need to correct the transport.

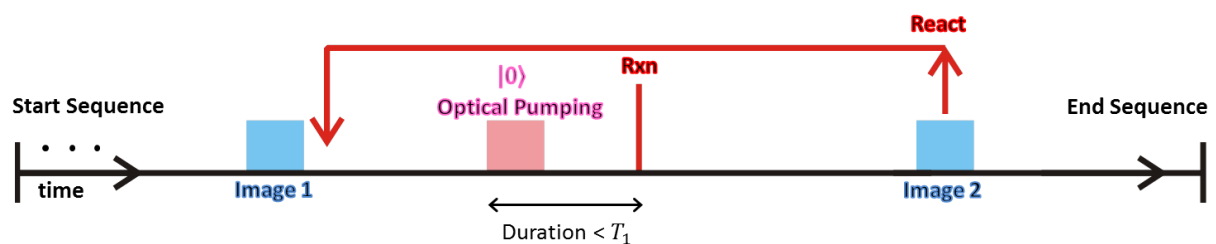


Figure 3.1: Single sequence containing reaction loops: A sequence begins by loading atoms into the lattice along with other preparatory procedures not illustrated in this diagram. The reaction loop consists of the inner operations and always begins and ends with taking an image. If the end result from Image 2 is satisfactory and no more reaction is required, the sequence proceeds to the end where the atoms are discarded and the laboratory setup is reset for a new sequence.

A typical experimental sequence involves several devices and programs to carry out operations (Fig. 3.2): the most important and central program is the Control Center—a self-programmed software that allows for user input through a graphical user interface (GUI) on the computer<sup>1</sup> [7]. The user has control over both the Control Center software as well as the camera software. The Control Center writes the output in the form of voltage signals to National Instruments (NI) multifunction data acquisition boards (NI PCIe-6259 and NI PCI-6723 cards) within the computer which have both analog and digital input and output channels connected directly to input ports of the MW generator, EOM, as well as the camera. Amplitude and frequency information is sent to the MW generator, voltage ramps corresponding to the lattice shifts are sent to the EOM, and a voltage trigger tells the camera to take an image. The image is then processed by the camera software which sends a message containing the number of atoms ("NUM") as well as a list of their positions in pixels ("POS") through what is called a Named Pipe [8] to the Control Center. From this information given by the image, the Control Center can decide how to react to write the new reactions to the NI cards.

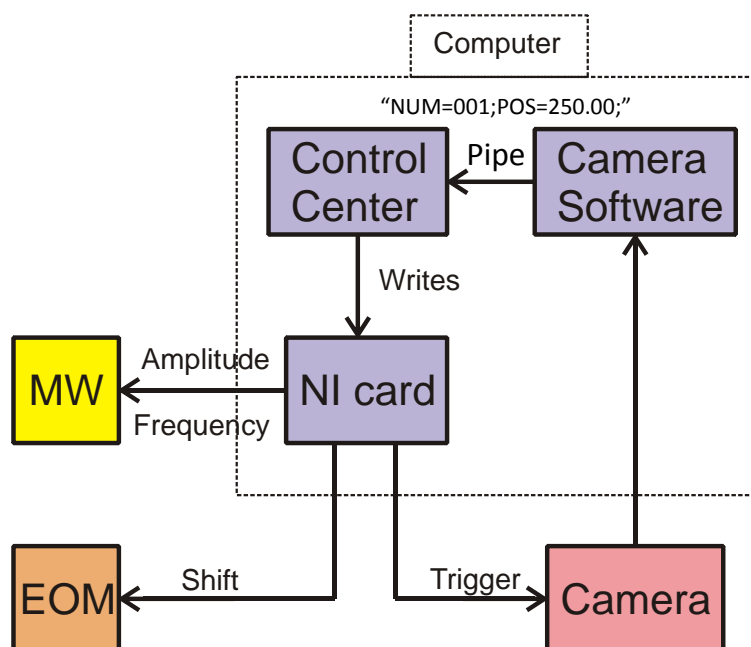


Figure 3.2: The main devices and programs behind transport: Within the computer is the Control Center, NI cards, and the camera software. The Control Center sends voltage signals through the NI cards directly to the MW, EOM, and the camera. The MW and EOM output depends on the reaction, which is determined by the Control Center upon analysis of a message from the camera that contains information about the number of atoms as well as their positions along the lattice.

In the next sections I will show exactly what those different reactions look like and will present results from experiments where we moved a single atom to an absolute target destination, as well as transported atom pairs together to a target separation.

<sup>1</sup> The Control Center software code was originally written in National Instruments LabWindows/CVI by former Ph.D. student Michal Karski but since then has been edited and added on to by Andreas Steffen and myself.

## 3.2 One Atom Movement to Target Position

### 3.2.1 Feedback Conditions

It is sound practice for a proof of principle experiment to perform basic tests successfully and then gradually add more complex features. Thus the first experiment was to move one atom to an absolute target position along the optical lattice. Naturally, we also tested and optimized all individual components of this basic experiment such as the communication between camera and Control Center as well as transport efficiency among other things.

The procedure follows the same feedback scheme from Fig. 3.1 but with specific conditions for which to react on an image or end the sequence right away. We loaded up to several atoms and our algorithm picked the atom closest to the target at 170.07 lattice sites as seen by the camera chip. The reaction for this particular experiment consisted of only state-dependent transport (see Fig. 3.3). The very first MW pulse in Fig. 3.3 to flip the atom to  $|1\rangle$  before the first EOM up ramp was optional and depended on whether we wanted the first movement to be to the right or left towards the target. Finally, the maximum allowed transport steps for *each reaction* between consecutive images, determined through observations of test runs and kept low to maintain high transport efficiency, was set to 20 transport steps = 10 lattice sites distance for a single atom. This means that for an atom farther than 10 lattice sites away it could only move maximally by 10 lattice sites at one time before having to take another imaged. And if closer, it would be transported directly to target.

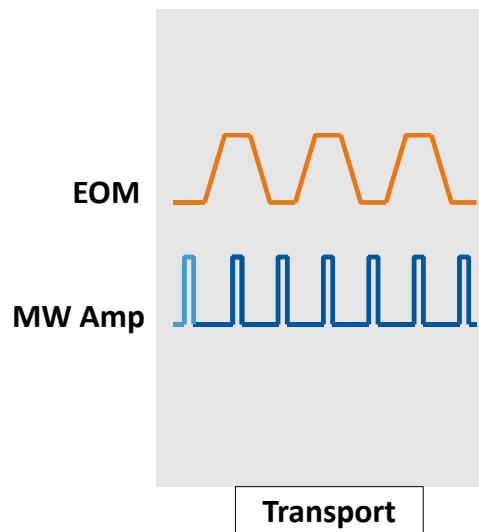


Figure 3.3: Transport reaction for single atom movement to target site: The curves are the voltage signals for the EOM ramps and MW amplitude of the pulses and follow the scheme described previously in Fig. 2.6 on pg. 8. The presence of the first MW pulse depends on right or left initial movement of the atom. The total number of steps (ramps and pulses) also depends on how far the atom is displaced from the target.

Determination for ending the sequence and no longer reacting was based on several conditions—whether there were no atoms loaded, too many atoms loaded so that the software could not detect their positions, atoms were too far from target ( $>50$  lattice sites meant that a set took a maximum of five reaction loops to get to the target), or an atom was directly on target (this could either come from coincidentally loading an atom there or from a successful transport reaction). What this meant for a reacting sequence was that we would react and take images until we lost the atom from the lattice or successfully moved it to target. The values of maximum steps per reaction as well as the maximum distance from

the target were chosen in order to produce a high success rate for our first set of measurements. Since the atoms were closer to the target, we took fewer transport steps to maintain high transport efficiency and fewer reactions and images to reduce atom losses in a sequence.

### 3.2.2 One Atom Results

We took two data sets for the one atom movement, each of which contained 120 total sequences, or new loading of atoms. Each sequence took anywhere between  $\sim 2\text{--}20$  s, mostly due to imaging time since a reaction is on a ms scale and much less than our  $T_1$  time of 200 ms. The time scale varied due to each sequence having a different number of transport steps as well as reactions and images. Overall, one data set took approximately 30 min which included the sequence time along with the time to edit and write new output to the NI cards.

Among each of the individual reactions, we observed transport successes, transport errors, atom losses, and finally atom jumps. Fig. 3.4, which contains an example sequence consisting of three reactions over four images, demonstrates both successes and jumps. The plot in Fig. 3.4 shows the selected atom's absolute position<sup>2</sup> as a function of the image number, with each corresponding image located below the plot. The boxed atom in the lower images follows the path in the plot connecting the points of "Actual positions" and eventually reaching its final destination at  $170.07 \pm 0.5$  lattice sites. The magenta points, or the "Should-be positions", are the positions that the atom should have moved based on its position from the preceding image. In this example sequence we start from Image 1 where the closest atom is at 175 lattice sites. In Image 2, the atom should have moved directly to the target in 10 transport steps (a movement of 5 lattice sites) since it was less than the maximum steps away. However, we see that in actuality, the atom jumped to the far left to 152 lattice sites. We know that it is a jump and not a transport error due to the following:

A transport error can occur for any combination of inefficient MW pulses that fail to flip the atom state. Under a transport error, the possible positions fall within a window starting from the "Should-be position" and ending on the opposite side of the original position. For example, if only the first MW pulse failed so that the atom began its transport in the wrong direction, if the remaining pulses were successful, the atom would end up completely in the opposite direction by the amount of lattice sites it *should* have taken to reach its target. The window in this case for the data point at Image 2 is  $175 \pm 5$  lattice sites. We can thus eliminate this as a transport error and conclude it as a jump (the inverse is not necessarily true since we cannot eliminate the possibility of a jump that occurs within the transport window). An atom jump is defined according to this strange behavior of the atom arbitrarily hopping to different, and often distantly separated lattice sites. We cannot attribute the cause of jumping at the moment, but we speculate that perhaps atoms that escape from the optical lattice are somehow recaptured in another site. Further experiments will be made to examine this behavior.

For the next reaction, the atom in Image 2 was supposed to move a maximal distance of 10 lattice sites to 162 lattice sites. And we see that in Image 3, the movement was correct and we count this as a success. Finally, the last image is another success and the sequence ends since the atom has reached the final target position.

---

<sup>2</sup> We leave out the error bars consisting of camera precision. They are  $< 0.02$  lattice sites and smaller than the actual data points.

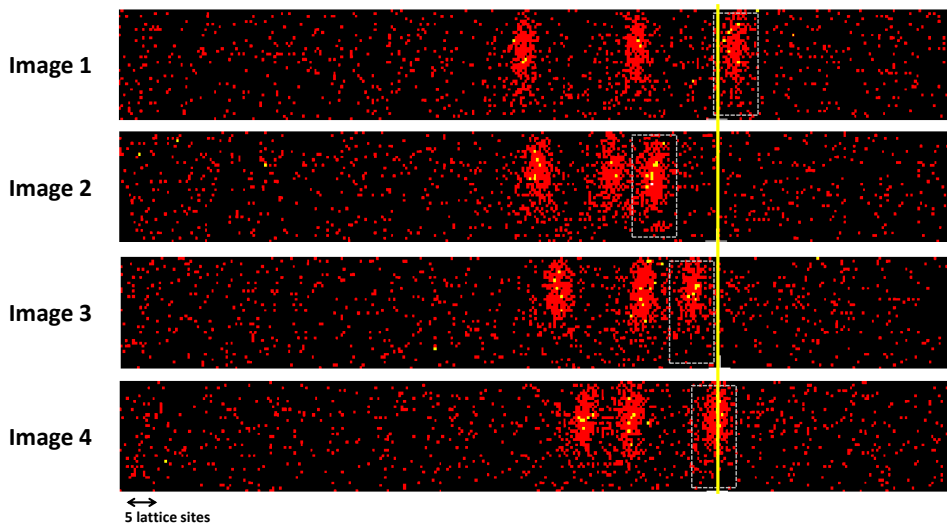
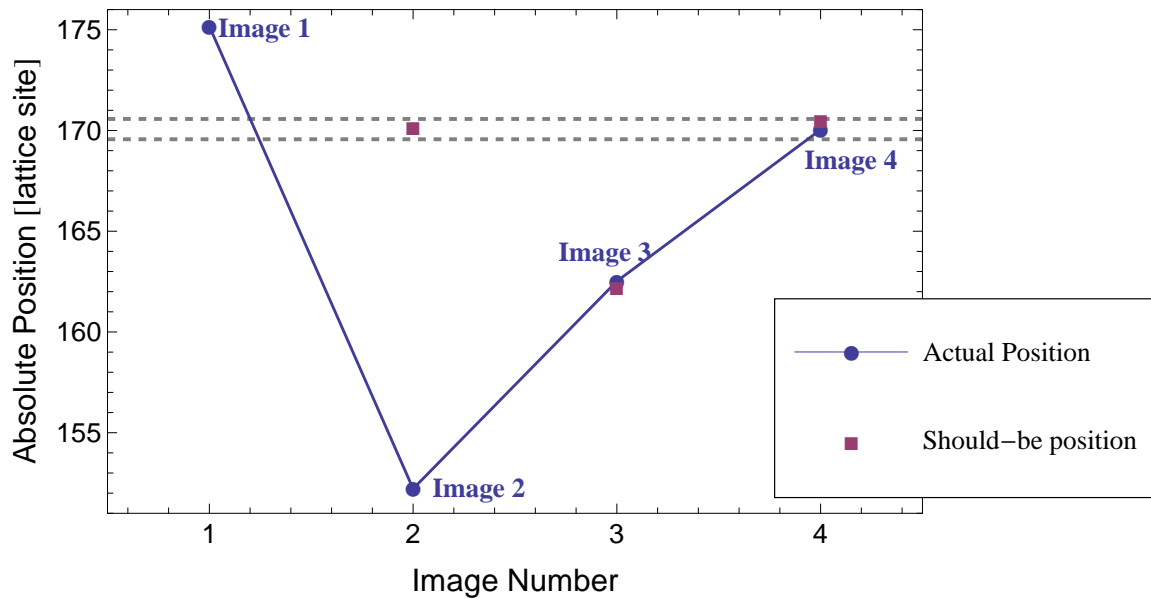


Figure 3.4: Example sequence demonstrating atom jumps and transport successes: Plot above: "Actual positions" are where the atom was in each image, and "Should-be positions" are where the atom *should* have been based on its position in the previous image. The dotted line region indicates the target region in which the last "Should-be position" falls. One can follow the "Actual positions" along with the image numbers in the camera images below. Camera images below: The solid yellow line indicates the target location and the dashed box surrounds the selected atom on which we base our reactions. The absolute position was chosen based on it being at the center of the camera field. But since the camera software utilizes a partial range of the chip, the target appears to be offset towards the right in subsequent images. A small scale below the images shows the approximate distance of 5 lattice sites. The behavior of the atom shows a jump in Image 2, far past the target. The remaining reactions are successful where the atom's "Actual position" is on the "Should-be position".

In the next example sequence (Fig. 3.5), one can additionally observe transport errors. In this sequence we only loaded one atom and had a total of six reactions within seven images. Transport to the target took more runs and although Images 2–4 show that the atom moved in the correct direction, these are all transport errors because the atom did not quite make it to its "Should-be position" until Images 5–7 where the points overlap.

The non-success of each reaction, even while only setting the maximum steps per reaction to 20, confirms the need for feedback and partial movements. At the same time, we do not want to take an infinite number of few-step reactions just to get to the target or else we waste time and increase the chance of losing the atoms during a long sequence or during imaging.

I now present the statistics for the two data sets. The pie charts in Fig. 3.6 display which behaviors were most prominent. The main differences between Data 1 and Data 2 are that Data 1 was the earlier set taken during the day where we first set the camera exposure time to 1 s. Data 2 was taken much later in the evening and was more susceptible to optics drifting. We set a shorter exposure time of 0.5 s since we noticed that we were losing many atoms. The percentages in the pie charts represent the results over all reactions (images) within all of the non-discarded sequences<sup>3</sup> with relative errors calculated using a binomial probability distribution [9]. This means that we look at the reaction occurring after every image (per data point in Fig. 3.4 for example) and not only the very end result. These measurements are more relevant because the majority of sequences in the data sets (both sets had > 65% transport success over all sequences) have eventually reached the target anyway. One should also keep in mind that for each reaction, there is a varying number of transport steps being taken and thus the presented statistics do not discern between reactions of different step numbers. Most of the reactions resulted in either successes or transport errors, with Data 2 having a lower success rate of  $28 \pm 2\%$  most likely due to the optics drifting over time. The jump rates are both low, although there is the possibility that this number is actually higher if some jumps occurred in the transport error window and so were tagged as transport errors. Finally, atom losses, which for this data set means the loss of the tagged atom, are also quite low and even smaller for Data 2 where the exposure time is cut in half to reduce losses. Overall, the statistics show that although there were a number of successful movements, there were also a significant number of transport errors occurring at some point during a reaction. Despite this finite aspect, we were still able to transport the atom to target by continuous application of feedback, as seen back in Fig. 3.5.

---

<sup>3</sup> The number of discarded sequences were different between the two data sets. the reasons for discarding sequences was discussed in Sec. 3.2.1

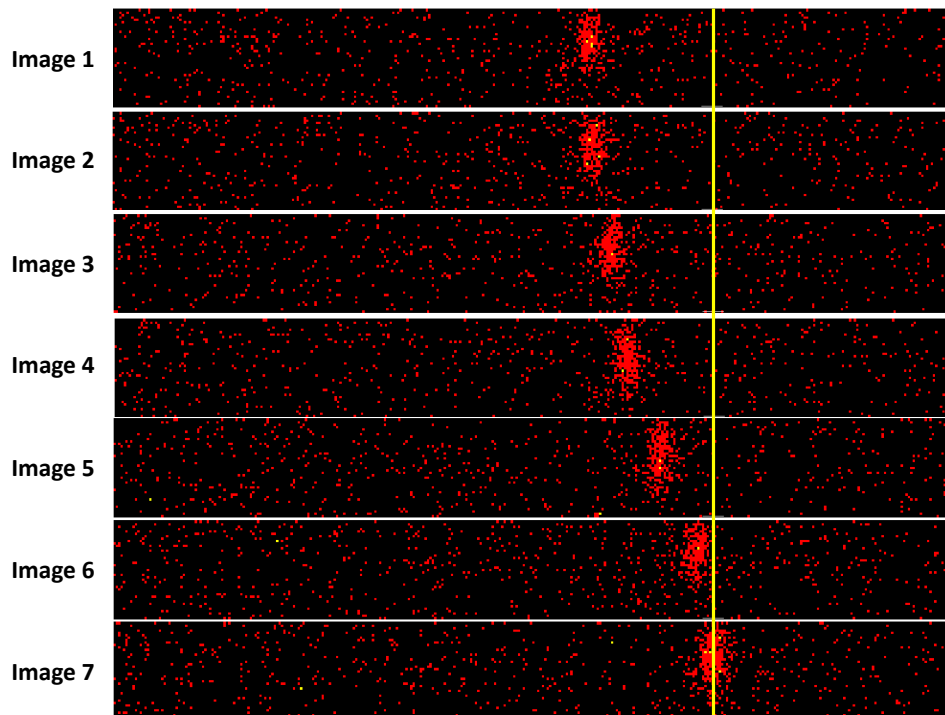
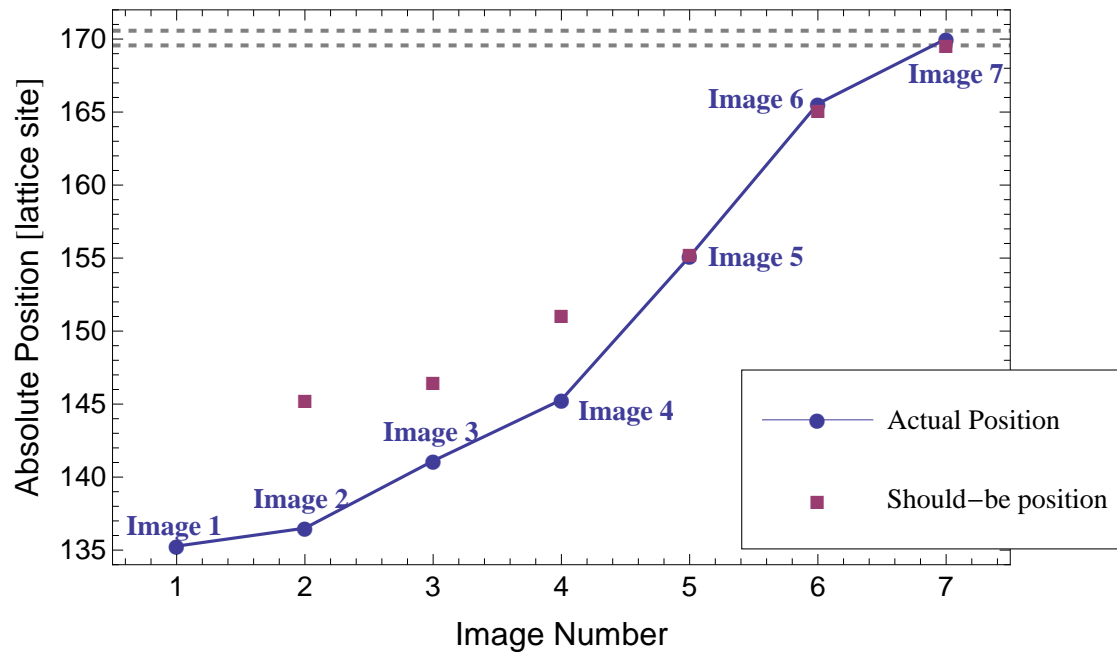


Figure 3.5: Example sequence demonstrating transport errors and successes: The plot and camera images follow the same structure as in Fig. 3.4. The behavior demonstrates transport errors all throughout images 2–4 and yet still move the atom in the correct direction. Images 5–7 are all successes.

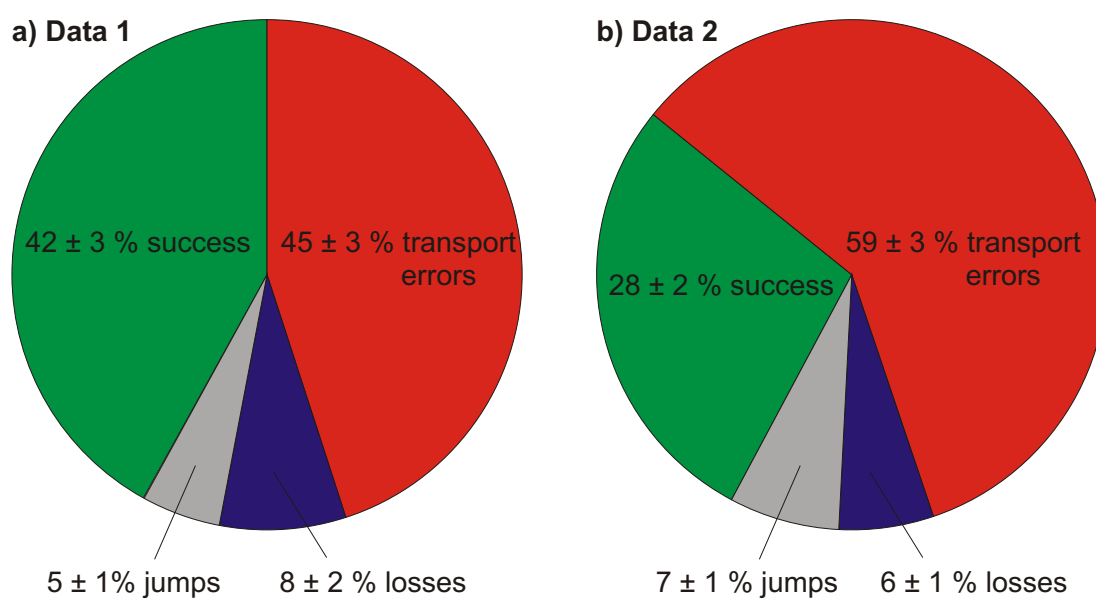


Figure 3.6: Transport successes and non-successes over all reactions in two data sets: (a) Data 1 had a 1 s exposure time. (b) Data 2 had a reduced exposure time of 0.5 s . For both data sets, of the non-successes, the highest contributor was transport errors from bad MW pulses. Jumps and selected atom losses have also contributed to a small percentage of the failures. These percentages are taken over individual reactions and do not differentiate between the number of transport steps taken in each reaction. That means that if an atom moves by 1 lattice sites in a reaction and makes it to the target, it is counted as a success. The same is the case if an atom moves by 10 lattice sites in a reaction.

Additional analysis on Data 1 and Data 2 is also shown in Table 3.1. First we have the efficiency per transport step  $P$ , that was calculated using only those reactions consisting of the maximum  $n=20$  steps<sup>4</sup>. Both values of  $94 \pm 3\%$  and  $92 \pm 3\%$ , although still quite high, are slightly lower than our achievable efficiency of 99% which means that we should be able to improve the success rate. The next parameter is the average number of atoms lost per reaction/image. This is different from the atom losses given in Fig. 3.6 because it counts *all* of the atoms lost between images. Interestingly, in the small percentages of reaction sequences where our selected atom was lost, we also lost all of the other atoms with it, indicating that perhaps there is a source which produced a collective effect on all of the atoms. This behavior cannot be explained yet and will also have to be analyzed further. Finally, the last three parameters in the table are the jumps among those sequences that have initially loaded 1 atom, 2 atoms, or greater than 3 atoms. These were measured because we wanted to see what effect the number of atoms had on the likelihood of a jump. And indeed, this makes a difference because the percentages increase with the number of atoms in the loaded sequence. To reduce the number of jumps in further experiments, we reduce the number of atoms so as to exhibit less erratic, jumping behavior.

Table 3.1: Other analysis taken over both data sets: The efficiency per step is comparable to our 99% from Fig. 2.8 on pg. 10. The average atom losses between imaging takes into account all of the atoms in a loading sequence and counts how many are lost per image. The jump rates for both data sets increase with the number of loaded atoms.

	Data 1	Data 2
efficiency per step	$94 \pm 3\%$	$92 \pm 3\%$
average atom losses between imaging	$6 \pm 1\%$	$5 \pm 1\%$
jumps (1 atom loading)	$2 \pm 1\%$	$3 \pm 1\%$
jumps (2 atoms loading)	$10 \pm 4\%$	$8 \pm 3\%$
jumps (>3 atoms loading)	$12 \pm 6\%$	$17 \pm 6\%$

Another visual representation of the overall data is shown in the plots of Fig. 3.7 (Data 1) and Fig. 3.8 (Data 2). The data points include all the successful reaction sequences that made it to the target destination while the entire plot shows the distribution of how many double transport steps it took to reach the target as a function of the atom's initial displacement. In principle, for a single atom initially displaced by 50 lattice sites, it should take 50 double steps to reach the target under perfect transport (in this case, we do not have any sequences with >50 lattice site displacement because these were filtered out as being too far from our target). Those points that fall on the dashed line bordering the triangle have undergone perfect transport and have reached the destination in exactly the number of steps required. The shaded region inside the triangle represents the possible region of transport and is where the majority of the data points lie. This indicates that it took more transport steps for those sets to get to the target (more steps to fix errors). There are also however, a few data points in both figures which fall below the perfect transport line and outside of the transport region. These sequences have reached the target in less steps required, thus demonstrating jumps. As expected, for small initial atom displacements from the target, there were less transport steps taken and less error corrections made so the points cluster about the transport line. The last trait to point out is that for Fig. 3.8, there are two outlier points which took  $\sim 135$  and  $\sim 180$  double transport steps to finally get to target. These two unyielding sequences demonstrate how robust the feedback and transport combination are and strengthen the argument for feedback.

<sup>4</sup> There were many of these reactions and thus provided a better statistical set

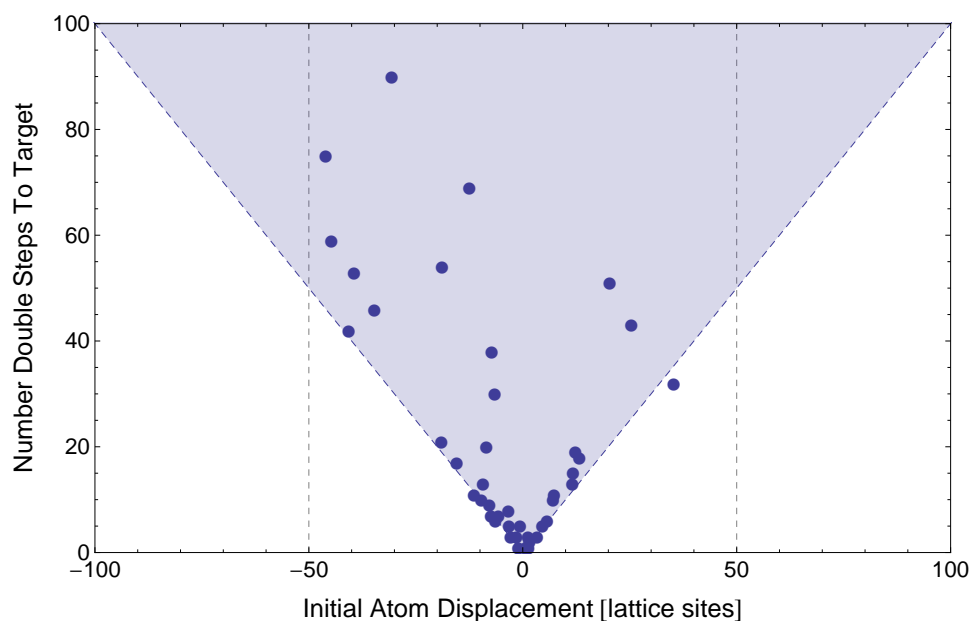


Figure 3.7: Successful reaction sequences of Data 1 and the number of double steps it took to reach the target: All of the data points are within 50 lattice sites initial displacement (as indicated by the vertical dashed lines). There are many points within the shaded region that took more double steps to reach the target, and some on the border which took exactly the number of steps corresponding to their initial distances. The few points outside the shaded, triangle region, result from jumps that brought them to the target in fewer transport steps.

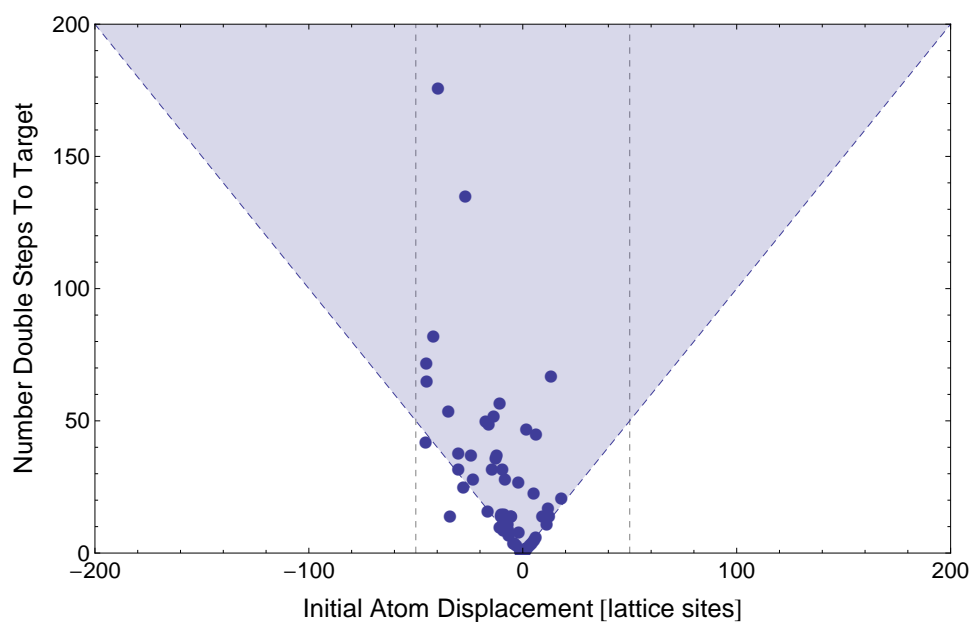


Figure 3.8: Successful reaction sequences of Data 2 and the number of double steps it took to reach the target: The plot is the same format as in Fig. 3.7. Note the two data points closest to the top of the plot. These are examples of those instances where it took many reaction repetitions to finally get to the target destination.

### 3.3 Bringing Two Atoms Together to Target Separation

The results from the single atom movement experiment have demonstrated a proof of principle as well as given valuable insight regarding the behavior of the atoms. The next series of experiments are more complex and bring us closer to being able to transport atoms together into the same lattice site. The basic idea is to bring two atoms closer together to a target separation and show that we can do this with a high success rate. The procedure is more complicated because we need to individually address atoms and flip their spins independent to the other atoms in the optical lattice. It is necessary for the two atoms to have opposite spins at one time in order for them to move towards each other (look back to Fig. 2.4 on pg. 6). The way to address specific atoms and flip their spin states is by applying a quadrupole magnetic field gradient which will change the resonance frequencies along the axis of the optical lattice. Thus, the transition frequencies of the Cs atoms become position-dependent due to a varying magnitude of the magnetic field strength and then we can address the atoms based on their positions.

#### 3.3.1 Magnetic Field Gradient Calibration

The quadrupole magnetic field gradient is produced by a pair of anti-Helmholtz configured coils which were mentioned previously in the experimental setup of Fig. 2.1 on pg. 3 and is directly proportional to the applied current to the coils. As we already know from Sec. 2.1, it is the strength of the magnetic field that determines the shift of the Zeeman levels within the  $F = 3$  and  $F = 4$  states, and hence the transition frequency between our qubit states. Furthermore, the energy spacing is directly proportional to the linearly increasing field strength along the lattice which means that the energy spacing also increasing along the lattice. From this we can obtain a frequency-position relation.

Under 9 A current delivered to the anti-Helmholtz coils, we applied a series of MW pulses of varying frequencies to a fully loaded lattice of atoms and measured the position of the dark regions where those addressed atoms in state  $|1\rangle$  were pushed out. The frequency scan resulted in the following (Fig. 3.9): A linear fit yields a frequency-position ratio of 2.5 kHz per lattice site. For this current strength, the coils require 26 ms of time after being turned off to proceed with operations: 6 ms for rise/fall time of the power supply producing the 9 A current, and 20 ms of settling time for the eddy currents to fully dissipate. This additional usage of time cuts away from our available reaction time. In principle, we can also increase the current to a maximum 45 A to obtain a larger ratio of 12.5 kHz per lattice site. But the downside for increasing gradient strengths is that the settling time grows as well.

With a calibration ratio of 2.5 kHz per lattice site, we can individually address the atoms by tuning our MW source to the frequency corresponding to the position. So far, we had been using rectangular MW pulses to flip the spins for transport. But as we saw in Fig. 2.7 on pg. 9, although they yield very high transfer efficiency, they are limited to a very narrow peak range and fluctuating wings on the outer edges. Thus, we offer an alternative via so called adiabatic passages, which have already been tested in our laboratories and used in the cavity QED experiments [10].

#### 3.3.2 Adiabatic Passages

Adiabatic passages are chirped MW  $\pi$ -pulses. While their basic operations are to transfer the atom between spin up and spin down states, their frequencies are not fixed and are swept over a larger range about the resonance frequency, resulting in a wider bandwidth and longer duration than for rectangular MW pulses. This slow frequency sweeping about the resonance is beneficial because it yields high population transfer as with the MW pulses but does not require the frequency to be exactly at resonance. We can see how this population transfer works using the Bloch sphere representation in Fig. 3.10.

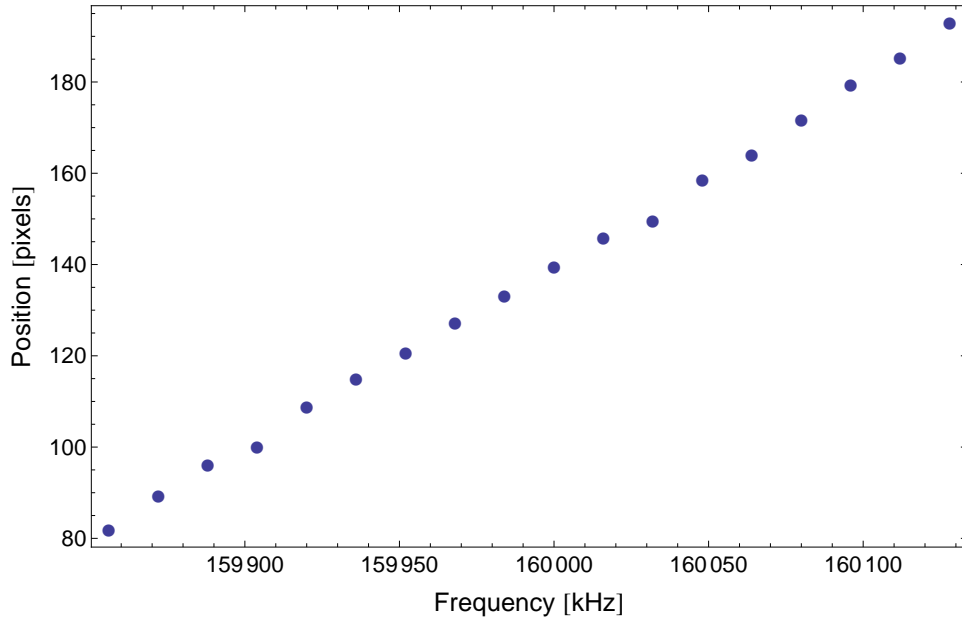


Figure 3.9: Linear calibration curve for frequency-position conversion: Under a 9 A current applied to the anti-Helmholtz coils to create a magnetic field gradient, we obtain a frequency gradient along the span of the optical lattice of 12.5 kHz per lattice site, which is just the inverse of the position vs. frequency slope.

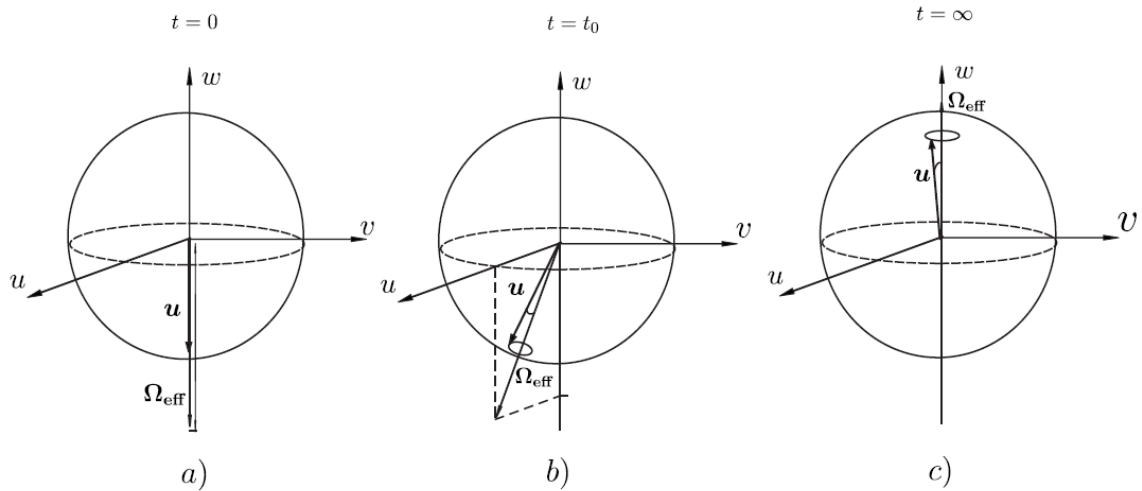


Figure 3.10: Evolution of the Bloch vector under application of an adiabatic passage: (a) At  $t = 0$ ,  $\mathbf{u}$  is in the ground state, or  $|1\rangle$ . (b) For  $t = t_0$ , as  $\Omega_{\text{eff}}$  rotates and crosses the resonance frequency,  $\mathbf{u}$  follows exactly while precessing around  $\Omega_{\text{eff}}$ . (c) At  $t = \infty$ ,  $\mathbf{u}$  has followed in  $\Omega_{\text{eff}}$  reversal to the excited state,  $|0\rangle$ . [11]

We have our Bloch vector  $\mathbf{u} = \langle u, v, w \rangle$  which describes the state of the 2-level atom as well as our torque vector  $\mathbf{\Omega}_{\text{eff}} = \langle \Omega_R, 0, -\delta \rangle$  of the external radiation field, where  $\Omega_R$  is the Rabi-frequency (basically the field amplitude) and  $\delta$  is the detuning frequency from resonance. We are reminded that the equation of motion given by  $\dot{\mathbf{u}} = [\mathbf{\Omega}_{\text{eff}} \times \mathbf{u}]$  describes the temporal evolution of the atom state under the radiative field and that the  $w$ -component of  $\mathbf{u}$  (called inversion) is the population difference between excited and ground states. Initially in Fig. 3.10,  $\mathbf{u}$  is in the ground state pointing down at  $\langle 0, 0, -1 \rangle$  along the same direction as  $\mathbf{\Omega}_{\text{eff}}$ . Then, at  $t = t_0$ , we start to slowly sweep  $\mathbf{\Omega}_{\text{eff}}$  (by changing its components, the Rabi-frequency,  $\Omega_R$  and detuning,  $\delta$ ) and  $\mathbf{u}$  begins to follow and precess around  $\mathbf{\Omega}_{\text{eff}}$  as it reverses direction. If this process is slow enough, then at the completion of  $\mathbf{\Omega}_{\text{eff}}$  reversal along the Bloch sphere,  $\mathbf{u}$  will have also flipped almost entirely to the excited state,  $\langle 0, 0, 1 \rangle$  as seen in Fig. 3.10c.

The adiabaticity condition which says that the effective torque vector,  $\mathbf{\Omega}_{\text{eff}}$  must be varied slowly enough for efficient population transfer is shown in the following [10]:

$$\frac{|\dot{\delta}(t)\Omega_R(t) - \dot{\Omega}_R(t)\delta(t)|}{2(\Omega_R(t)^2 + \delta(t)^2)^{3/2}} \ll 1 \quad (3.1)$$

It basically requires that the variation of both  $\delta(t)$  and  $\Omega_R(t)$  be small enough. The form of these functions that fulfill this condition and have also been successful in our cavity QED experiments [10] are the following:

$$\begin{aligned} \Omega_R(t) &= \Omega_{\text{max}} \sin^2(\pi t/t_p), \\ \delta(t) &= \delta_c + \text{sgn}(t - t_p/2)\delta_{\text{max}} \sqrt{1 - \sin^4(\pi t/t_p)} \end{aligned} \quad (3.2)$$

for  $0 < t < t_p$ .  $\Omega_{\text{max}}$  is the maximum possible Rabi-frequency,  $t_p$  is the adiabatic passage pulse duration,  $\delta_c$  is the central detuning or the central resonance frequency (which for simulation purposes is simply set to zero), and  $\delta_{\text{max}}$  is half of the entire frequency sweep span. Using the following values for the simulation, the functional form of our adiabatic passages is given in Fig. 3.11:

$$\begin{aligned} \Omega_{\text{max}}/2\pi &= 50\text{kHz} \\ t_p &= 1\text{ms} \\ \delta_c &= 0 \\ \delta_{\text{max}}/2\pi &= 25\text{kHz} \end{aligned} \quad (3.3)$$

The plots in Fig. 3.11 are  $\Omega_R(t)$ , the MW amplitude as a function of time, and below is  $\delta(t)$ . Both the amplitude and frequency plots have a width and total duration of  $t_p$ . If we follow both curves together, we can see that the amplitude is at its maximum when we are at zero detuning (at resonance frequency) and then becomes weaker towards the edges of the frequency sweep.

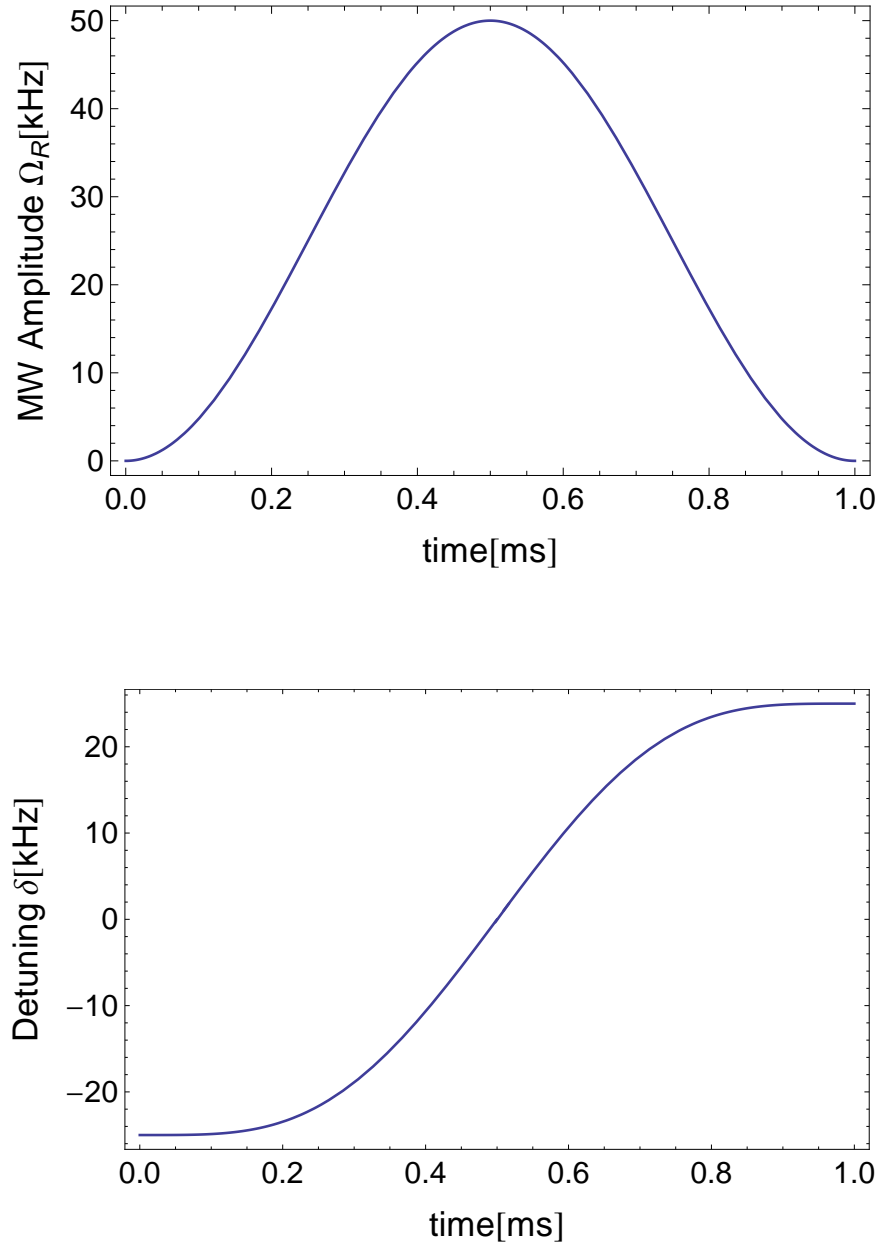


Figure 3.11: Adiabatic passage functional forms for the amplitude and frequency, as given by Eq. (3.2): The top plot is the MW amplitude function,  $\Omega_R(t)$ . Below is the  $\delta(t)$  function. Both plots were simulated using the values from Eq. (3.3) and exhibit slowly varying behavior to maintain adiabaticity.

Using the functional forms given in Eq. (3.2) as well as the parameters in Eq. (3.3), and solving  $\dot{\mathbf{u}} = [\mathbf{\Omega}_{\text{eff}} \times \mathbf{u}]$  for  $\mathbf{u}$ , we obtain a numerical solution for the  $w$ -component describing the population difference. The simulation can be seen in Fig. 3.12. The transfer efficiency curve gives almost unity or 100% efficiency all throughout a plateau width of  $\sim 2\delta_{\text{max}}$  (this corresponds to 50 kHz for the simulation). At the edges of the frequency window, the efficiency drops very sharply and is zero everywhere outside. The overall shape makes these adiabatic passages very robust and forgiving on a tunable range of detunings (the parameters can be tuned and adjusted to produce a desired output). The transition behavior between almost perfect efficiency and zero transfer is sharp. This effect is beneficial for when we use the magnetic field gradient to address atoms of different frequencies because it allows us to be precise over which atoms should be flipped completely and which should not be affected at all by edge remnants in the spectrum as seen back in Fig. 2.7 on pg. 9.

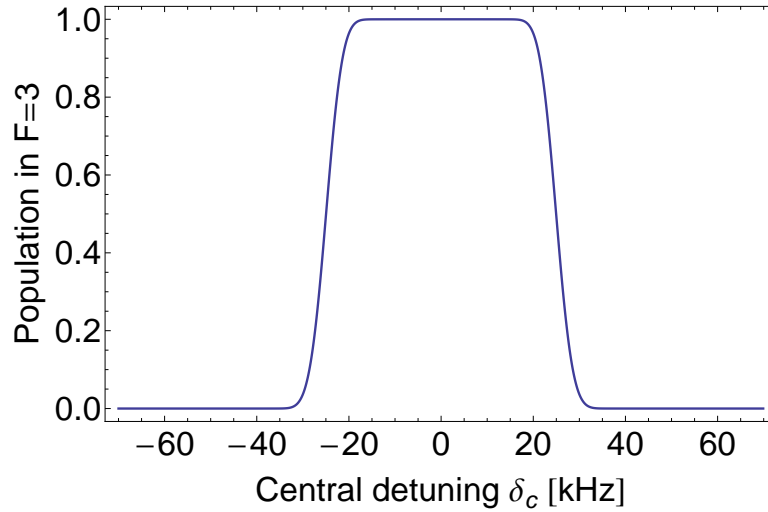


Figure 3.12: Numerically simulated population transfer plot for adiabatic passages with experimental parameters given in Eq. (3.3): The graph shows the population in  $F = 3$  as a function of the central detuning frequency (in this plot, our atomic resonance is at  $\delta_c=0$  kHz). The efficiency is almost 100% over a window range of 50 kHz. Elsewhere outside the window, the transfer probability is zero.

So far I have shown a simulation with high population transfer within a window of 50 kHz. Increasing the frequency sweep easily widens this window while maintaining good efficiency. We can also tune a narrow window and smaller frequency sweep as seen in the simulation curves of Fig. 3.13. The three curves were simulated with  $\delta_{\text{max}}=12.5/2$  kHz so that the width of the window would cover 12.5 kHz, the frequency width of one lattice site under a maximum magnetic field gradient. However, because the sweep range is drastically reduced, the pulse duration must compensate and increase to maintain the adiabaticity condition from Eq. (3.1). Plots (a), (b), and (c), use durations of  $t_p=1, 2,$  and  $5$  ms. The curves improve with increasing  $t_p$  and otherwise for very short pulse times, display no plateau and have gradually decreasing edges. We can see that if we want to tune our adiabatic passages to get within a single lattice site, we need to apply a maximum gradient as well as increase the pulse time.

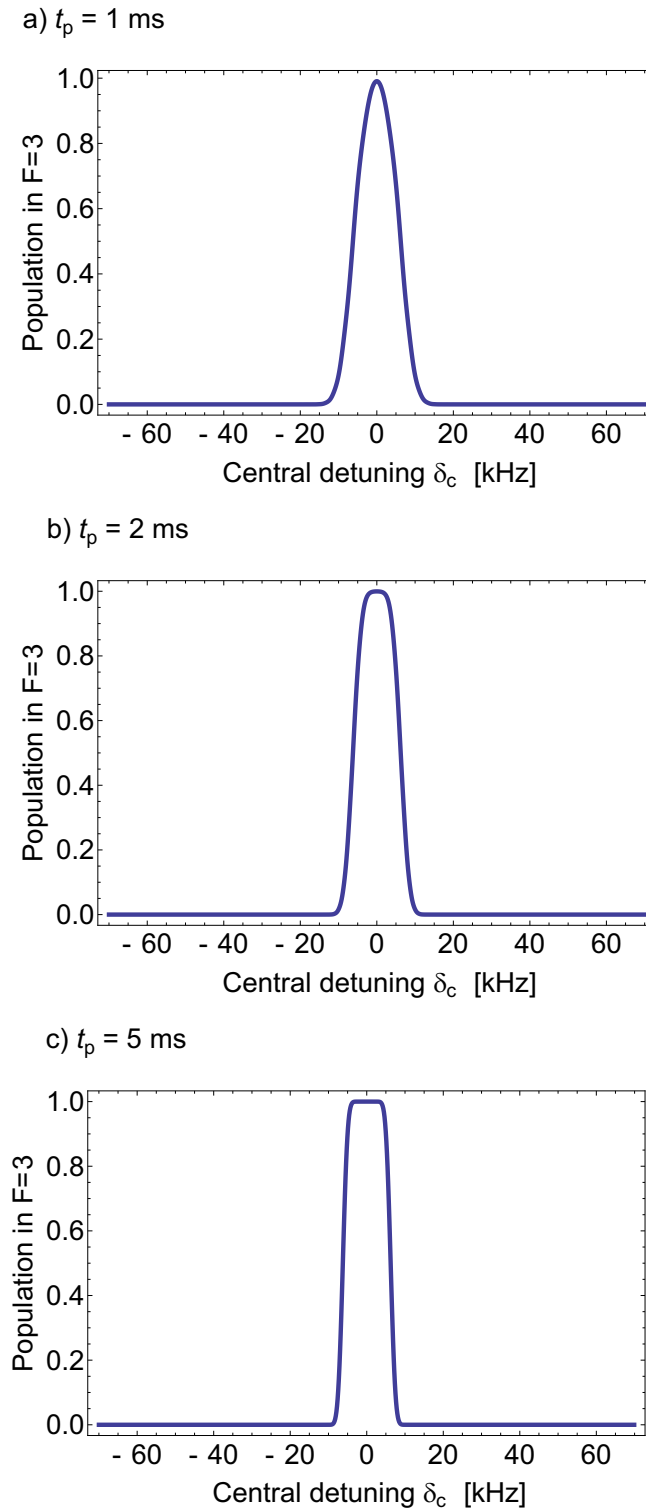


Figure 3.13: Population transfer efficiency curves of  $\delta_{\max}=12.5/2$  kHz (to give a window width corresponding to one lattice site distance in frequency) and varying pulse times: (a)  $t_p=1$  ms, (b)  $t_p=2$  ms, (c)  $t_p=5$  ms. Increased pulse time improves the quality of the curves which have been drastically narrowed as compared to the curve from Fig. 3.12 with 50 kHz bandwidth.

By adjusting the various parameters, all while maintaining the adiabaticity condition, we can tune the frequency width of the adiabatic passages and select which atoms we want to address along the optical lattice. This tunability allows us to optimize two atom transport as illustrated in Fig. 3.14. The blue boxes represent the windows of our adiabatic passages, and simultaneously span position and frequency (due to our position-dependent frequencies). The schematic shows the different scenarios for transporting two opposite spin atoms together and how we can tune our adiabatic passages to address and flip the states of the atoms. When the atoms are far away from each other (Fig. 3.14a), we can use a relatively wide pulse of short duration to achieve high transfer. When they are situated a bit closer (Fig. 3.14b), we reduce the window as to not affect the other atom. Finally, when the atoms are very close or at neighboring sites, we have the choice of either widening the pulse to flip the states of both atoms so that we can move them apart and retry to bring them directly together into the same lattice site (Fig. 3.14c), or tuning the pulse to be very narrow to address each individual atom (Fig. 3.14d). The last configuration is the trickiest scenario because it requires high precision. As an alternative, one could also control the strength of the magnetic field gradient as this has the same effect as tuning the frequency bandwidth of the pulse.

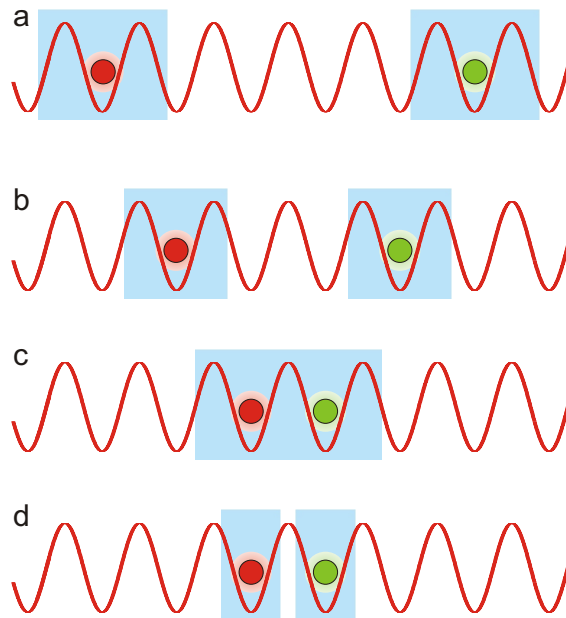


Figure 3.14: Adiabatic passages with tunable bandwidths for the different cases to bring two atoms together: (a) atoms far away: use wide pulse with short duration. (b) atoms a bit closer: use less wide window range. (c) atoms very close or neighbors: use a wide window to cover both atoms in order to move them apart and retry to bring them into the target configuration. (d) atoms very close or neighbors: the other option is to make pulses very narrow with a longer duration to address individual atoms.

### 3.3.3 Feedback Conditions

The reaction procedure for the two atom movement to a target separation is different from the transport procedure for the single atom movement because there are two additional operations that occur before transport. The procedure can be seen in Fig. 3.15. For the addition of adiabatic passages, a separate signal is required for MW frequency modulation on top of the MW amplitude. Additionally, there is now a magnetic field gradient.

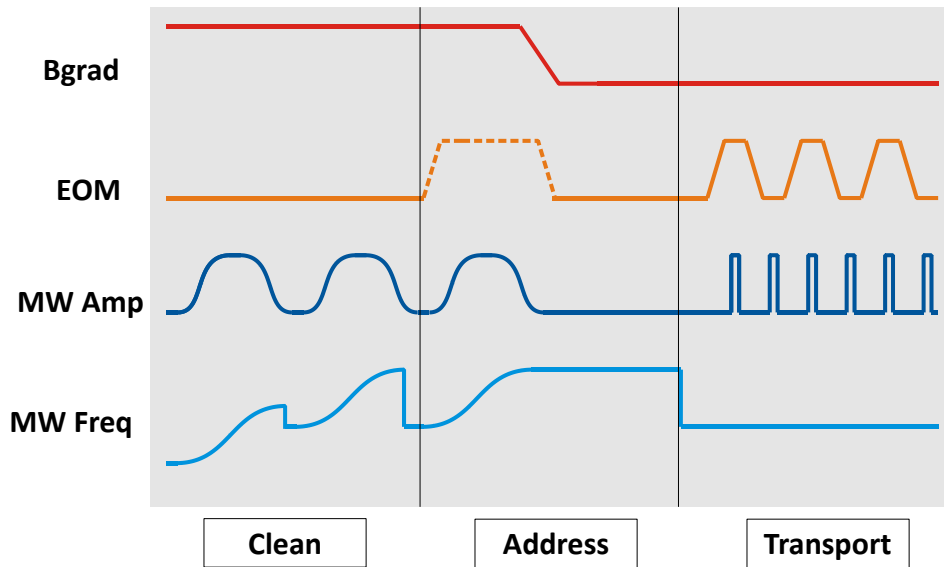


Figure 3.15: Reaction procedure for bringing two atoms to target separation: Like the scheme back in Fig. 3.3 on pg. 13, the main devices are listed on the left side with the new additions of MW Freq and Bgrad. The clean procedure selects an isolated atom pair and initializes their states by applying two consecutive adiabatic passages, all while the magnetic field gradient is on. Depending on the positions of the selected atoms, their central frequency offset as well as the sweep range will be different. All other remaining atoms are then pushed out. If the clean is successful and there are two atoms in the next image, an address and transport sequence is applied. First, one atom is spin-flipped by an adiabatic passage so that the two atoms have opposite spins. Then, the gradient is ramped down for normal transport where we apply the standard MW pulses to flip the spins of both atoms. This way, the atoms of opposite spin will move towards each other with each transport step. Finally, the EOM double ramp in address is optional and is used to change the transport from odd steps to even.

The three parts—clean, address, and transport demonstrate different operations. Cleaning means selecting an atom pair which is isolated from all the other atoms in a new loading, and then applying the push-out procedure to the remaining, unwanted atoms. The procedure arranges starting configurations where we can select which atoms to keep for following operations. This reduces the number of atoms in a set and therefore reduces jumps as seen in the single atom experiments. Cleaning atoms also makes analysis clearer since we can track the movements of atoms which are farther apart from each other. When atoms are too close, it is sometimes difficult to discern in the next image which atom moved where. A cleaning operation is done by first applying a simple algorithm that compares the atom separations and chooses the two atoms that have the greatest separation distances from a neighbor. The control center then addresses the two selected atoms under a magnetic field gradient by applying two tuned adiabatic passages. The adiabatic passage detuning frequencies are set based on the atoms' positions and the sweep ranges based on the separations. This way, we avoid affecting neighboring atoms.

but at the same time keep enough room for frequency drifts (in the case that the lattice or the gradient drifts). The selected atoms are then spin-flipped into the  $|0\rangle$  state.

The next column in Fig. 3.15, the address procedure, involves the addressing of one atom to flip it to the opposite spin to precede two atom transport towards a target separation. The dotted line indicating an up-down EOM ramp is optional and will be discussed later. An adiabatic passage is applied, followed immediately by a ramp down of the magnetic field gradient, to allow for settling time.

The last column is just standard transport with our normal, rectangular MW pulses (so no MW frequency signal) with the first pulse omitted since the spin flip is covered in the address operation. As with the single atom movement, the number of transport steps varies depending on how far the two atoms are from their target separation. Another important aspect to take into account is the fact that for two atoms, 1 transport step moves them together by 1 lattice site distance. This means that for the even step requirement between imaging, the atoms can only move by an even number of lattice sites, which can pose as a problem if the two atoms need to move by an odd number of sites. To solve this problem, we utilize the optional EOM double ramp in addressing. The up ramp portion shifts the lattice without displacing the atoms at all (since they have not been flipped yet to opposite spins). The down ramp then shifts the two atoms by one lattice site following the adiabatic passage. Thus, an additional one lattice site is added onto the atoms' movement plus a remaining even number of transport steps set in the transport column.

For a single reaction (consisting of two images), either the cleaning operation exists alone, or the address and transport occur together without the cleaning. This way, we can repeat cleaning if we do not clean enough atoms in the first try. If then the clean succeeds, we proceed with an address and transport operation and reapply until the final goal is reached.

### 3.3.4 Determination of Maximum Steps

The maximum number of steps per reaction was chosen to be 50 transport steps, corresponding to 50 lattice sites distance for the two atoms together. This was chosen from observing several test runs and shown to yield a high success rate. However, a more precise value for the maximum steps can be determined to optimize our transport if we follow the movement of an atom's average displacement while taking into account that the direction it moves depends on the state it is during an EOM shift.

To save time as well as to avoid many reactions and imaging, we would like to transport our atoms directly to the target. We are, however, limited by the transport efficiency from Fig. 2.8 and we see that the success drops exponentially with an increasing number of transport steps. This curve only gives us an idea of how likely it is that our atom ends up exactly in the lattice site where we intend to transport it; it does not tell us where unsuccessful movements take the atom. We are interested in the latter to set the maximum transport steps per reaction as large as possible so to minimize the number of feedback reactions. For example, if we want to move the atom over a far distance and are not so concerned with being exactly on target, then we can apply the maximum number of steps to move the atom significantly closer. Then, if the atom is at a closer distance for which the target can be precisely reached, we transport directly and can also apply operations for fixing odd/even transport steps.

The following recursion relation illustrates the average movement of a single atom given a finite probability to transport along the correct direction:

$$x_{n+1} = P(1 + x_n) + (1 - P)(-1)(1 + x_n) \quad (3.4)$$

with the initial condition of  $x_0 = 0$  where  $x_n$  and  $x_{n+1}$  are the average displacements in lattice sites

from the start (the origin is at 0) and  $n = 0, 1, 2, \dots$  is the number of double transport steps<sup>5</sup>.  $P$  is the probability of successful movement in the correct direction, which is exactly the probability of the addressing pulse. In formulating Eq. (3.4), we assign the correct initial path to be 1 lattice site to the right on the first transport step, as indicated by  $(1 + x_n)$ . The two terms in Eq. (3.4) both include this displacement factor but can be differentiated by their factors of  $P$  and  $(1 - P)$ . The second,  $(1 - P)(-1)(1 + x_n)$ , as opposed to the first term, represents the displacement for a transport fail, given by the probability  $(1 - P)$ . The remaining term factor of  $(-1)(1 + x_n)$  indicates that the movement direction during step  $n + 1$  is exactly opposite to the direction during step  $n$ . For example, if  $P = 0$  so that we have definite probability for a failed spin flip, only the second term would remain and the resulting behavior would be  $x_0 = 0, x_1 = -1, x_3 = 0, \dots$  so that the atom fluctuates back and forth about the origin without moving anywhere at all. This is exactly the behavior of an atom that keeps the same state while the EOM shifts the lattice back and forth. On the other hand, if there is perfect transport,  $P = 1$ , then the atom will be displaced exactly with  $n$  and the relation will be linear. If then  $P = 1/2$ , the average displacement will always be zero regardless of  $n$ . A plot of  $x_n$  as function of  $n$ , can be seen in Fig. 3.16 as the solid blue curve where  $P = 99\%$  for the simulation.

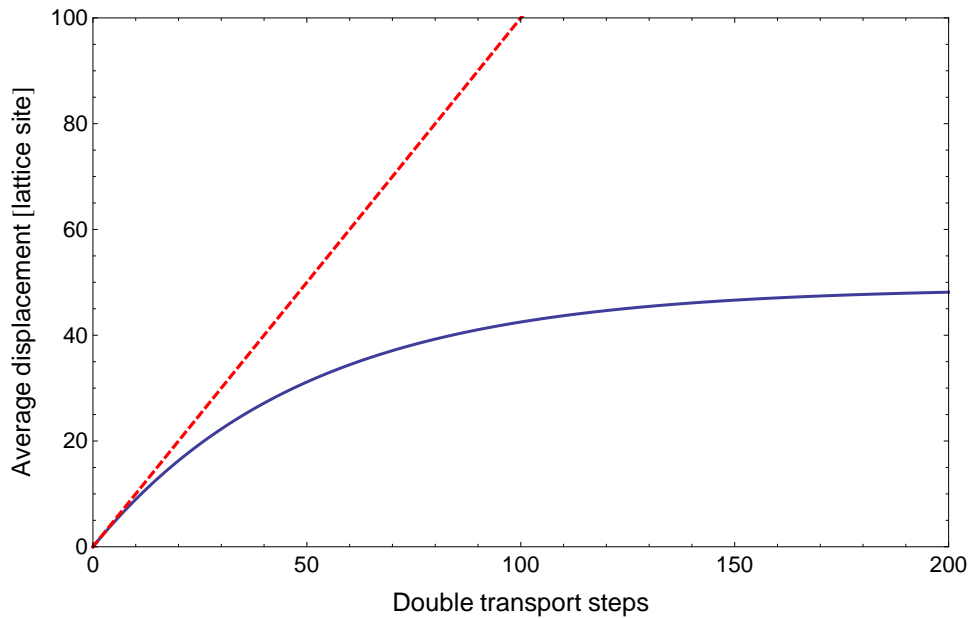


Figure 3.16: Plot to determine the average displacement of an atom under a finite probability: The solid blue curve is the position displacement as a function of the number of double transport steps (Eq. (3.4)) for  $P = 99\%$ .  $P = 100\%$  is the dashed red line and indicates perfect transport efficiency. The two curves overlap until around  $n = 20$  at which point the atom moves very slowly towards the correct direction. A limit of 50 lattice sites average displacement occurring at approximately  $n = 100$  indicates that we should not apply more than 100 double steps per atom since the average movement will not change.

While the solid curve shows an atom's actual movement under double transport steps, the dashed red line shows perfect transport of a displacement equal to the number of transport steps (the  $P = 1$  case as described above). The overlap of the two curves is quite good until 10–20 double steps and then the atom is less likely to move by the full distance required. Then from 20–100 double steps, we see that the atom approaches the correct direction but at a much slower rate. From 100–200, the curve slowly approaches an asymptote of 40–50 lattice sites displacement. This means, that there is no use in going

<sup>5</sup> As a reminder, one atom moves by  $1/2$  lattice site per transport step—one site per double step

beyond 100 double steps because the atom will move by only 50 sites on average. Past 200 double steps is irrelevant because this takes us beyond our limited  $T_1$  time. For future experiments, we can thus assign the maximum transport steps to 100 double steps for each atom to be transported at one time. We can also choose 20 double steps to be the maximum steps where we fix the odd/even transport. This distance yields a high likelihood of transporting directly to the target and is thus worth applying the optional EOM ramp that was seen in Fig. 3.15.

### 3.3.5 Two Atom Results

The most recent results from the two atom experiments are presented here for two sets of data, Data 3 (where the target separation was set to 10 lattice sites) and Data 4 (target separation even closer at 4 lattice sites). We look at how successful the cleans were as well as the address and transports. But first, we look at Fig. 3.17 at the spectrum of our adiabatic passages to confirm the efficiency predicted by the simulation curve from Fig. 3.12 on pg. 25. The spectrum was taken for  $t_p=0.5$  ms,  $\delta_{\max}/2\pi=50$  kHz, and an amplitude of  $\Omega_{\max}/2\pi=25$  kHz with approximately 95% transfer efficiency. And indeed, there is a plateau at high efficiency while the outside of the window is almost zero.

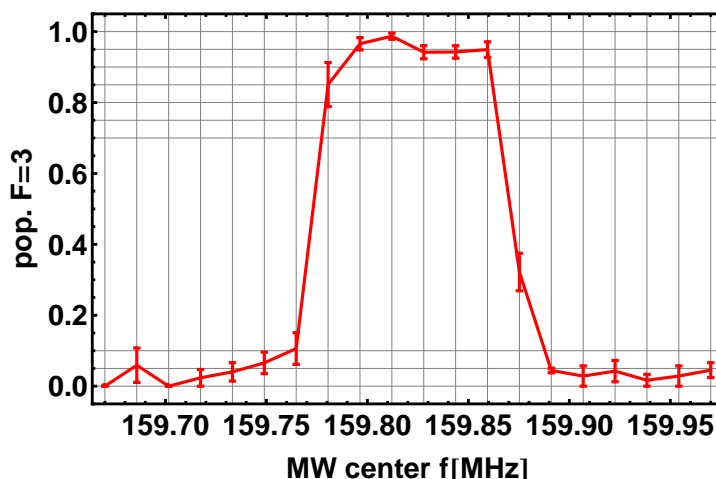


Figure 3.17: Adiabatic passage spectrum from experiment: The curve for population transfer efficiency looks very similar to the simulation from Fig. 3.12 on pg. 25. This pulse corresponds to a window width of 50 kHz.

Example images from successful reactions can be seen also in Fig. 3.18 for Data 3 and Fig. 3.19 for Data 4. Fig. 3.18a begins with a loading of five atoms, two of which on the right-hand side have overlapping fluorescence regions. The atoms are cleaned and the two outermost atoms remain in Fig. 3.19b. Although the cleaning worked and left two isolated atoms, the selection of the right atom did not correctly follow the cleaning algorithm which tries to avoid selecting atoms that are too close to one another. The next images (b)–(g) show the result of the address and transport procedures. We can see the outcome of the transport in the images, but unfortunately cannot discern any information regarding the addressing portion. Nevertheless, six total applications of address and transport take the cleaned atoms to the target separation of 10 lattice sites.

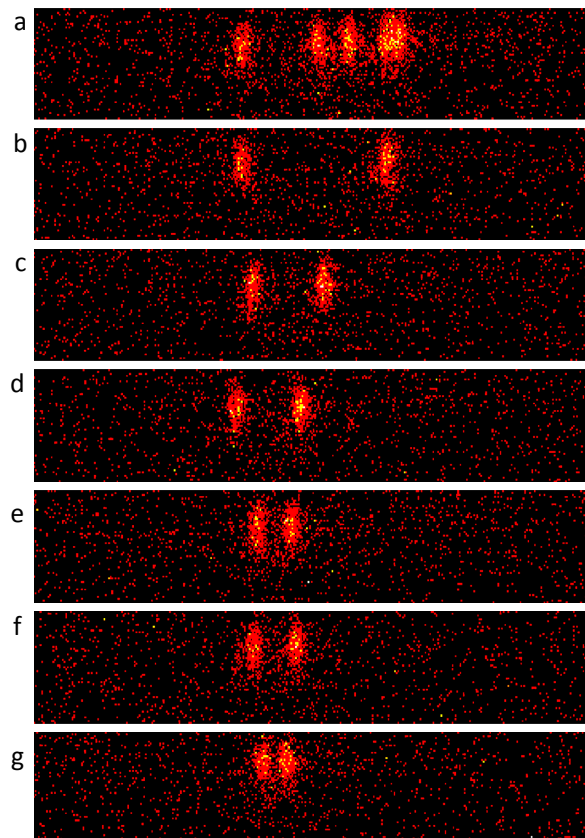


Figure 3.18: Images of a successful sequence from Data 3: (a) In the initial image where there are five atoms loaded, a reaction consisting of cleaning takes place. (b)–(g): Since cleaning is successful, the following reactions consist of only address and transport until the final target separation is achieved.

The next series of images in Fig. 3.19 come from a successful sequence of bringing the atoms to a separation of 4 lattice sites. From a loading of five atoms, the isolated pair remains in (b). It takes several tries but they are eventually brought together by Fig. 3.19g.

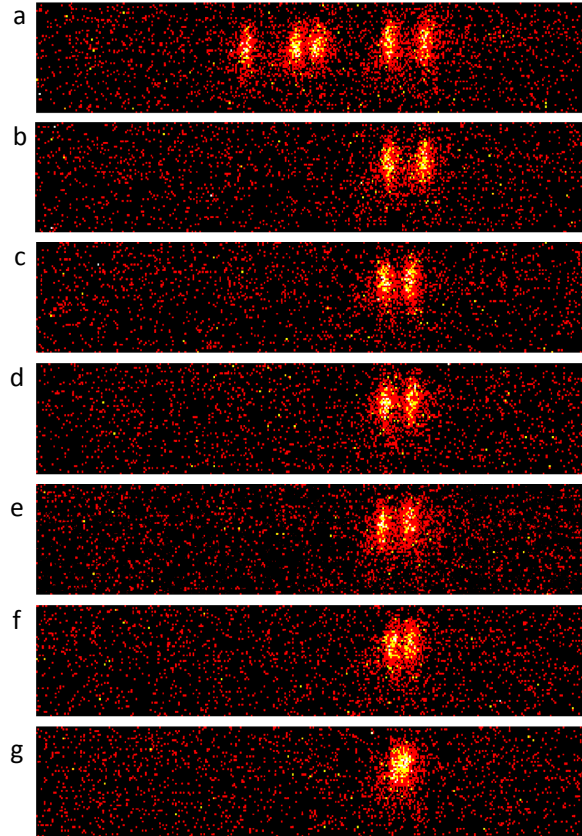


Figure 3.19: Successful sequence from Data 4: (a) From a loading of five atoms, the rightmost pair is selected during the clean and all other atoms pushed out. (b)–(g) The reaction images end when the two atoms are 4 lattice sites apart.

We finally arrive at the numerical analysis to get an idea of how successful each cleaning attempt and each address and transport really was. Fig. 3.20 contains two pie charts from Data 3 and Data 4 showing the percentages of successful cleans out of all possible attempts. The different portions of the pie chart are indicated by the colored legend. "Cleaned both" means that the cleaning was perfect and that the two atoms selected by the Control Center remain in the next picture. For the two data sets, this percentage (15%, and 20%) is somewhat low so we know that we must improve our cleaning procedure. For those reactions where the clean was not perfect, "cleaned 1" dominated. This means that in the subsequent image, only one of the atoms was present, and the other had been cleaned out and removed with the rest. The next, "cleaned none, lost all atoms", are those reactions with images that had no atoms remaining after a clean attempt. "Cleaned none, wrong atoms remain" include those reactions where there were one or more atoms remaining but not the correct selected ones. This value makes up a large amount of the total attempts. Finally, "too many atoms left", refers to there being more than 2 atoms remaining after a clean. From further observation, all of these cases have shown there to be 3 atoms remaining, half of those cases contained one of the selected atoms, and the other half contained both selected atoms. It was often the case that an attempt was made to clean, but three atoms were left because one atom was very close to one of the selected ones and thus difficult to get

rid of (it was addressed along with the selected atom). In the next image, the Control Center tried to clean again and failed another time for the same reason until at some point the atoms were all lost. What can be said overall regarding the cleaning procedure, is that even with a high population transfer as demonstrated by the adiabatic passage spectrum, and an efficient push-out of  $96 \pm 2\%$ , work still needs to be done to improve the cleaning fidelity. We did several simpler experiments before these two data sets, including a few that only executed the cleaning procedure. The effect was much better in these sets and unexpectedly dropped in performance afterwards. Between the two data sets, we had to realign the lattice beam overlap which might have been a source behind the decreased performance. Perhaps the selection algorithm can be designed to be more precise, or we can test the robustness of two consecutive adiabatic passages for addressing. The details will be looked into further since the applications of cleaning are important not only for this experiment, but also the quantum walks experiments.

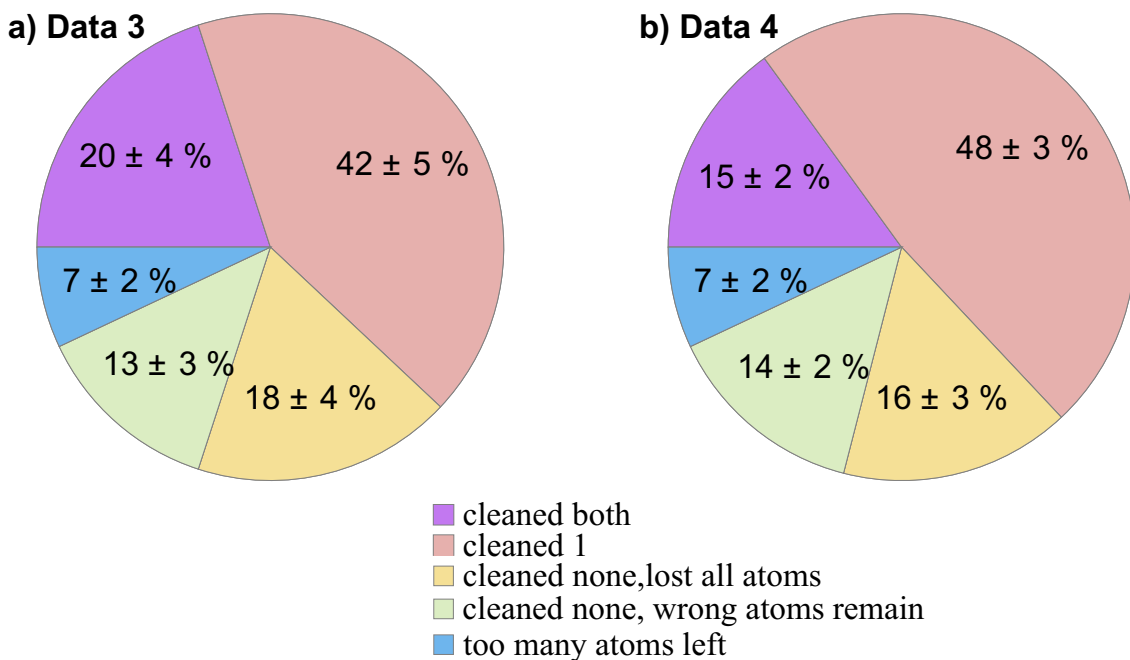


Figure 3.20: Results over all clean attempts in Data 3 and Data 4. The majority is dominated by "cleaned 1" behavior. This means that most of the cleaning attempts were only able to keep one of the selected atoms and not both.

Although the cleaning procedure has been demonstrated, it needs to be improved to provide consistent success. On the other hand, there is also the address and transport part of the reaction. Data 3 was calculated to have  $40 \pm 7\%$  success over all sequences, and Data 4 had a higher success rate of  $62 \pm 5\%$  most likely due to a recalibration of the transport MW pulse between the two measurement sets. The address and transport behavior was successful and reflected the transport behavior of the one atom measurements. For the two atom measurements however, we saw less jumps, most likely due to only having to transport two atoms. Most of the non-successes were due to atom losses.

The successful transport sequences that reached the target separation can be seen in Fig. 3.21 for Data 3 and Fig. 3.22 for Data 4. The two plots illustrate the same idea as the plots back in the one atom movement measurements (Fig. 3.7 on pg. 20). Fig. 3.21 contains less data points than Fig. 3.22 because there were more cases of discarded sequences of atoms that were closer than the target separation of 10 lattice sites. Although there were sequences demonstrating perfect address and transport (those points that fell directly on the dashed line), most sets took more transport steps to get to the final orientation. Finally, we also see that there are no points that fall below this perfect transport line, so no atom jumps towards the target direction.

Two atom transport towards a target separation of down to 4 lattice sites has been demonstrated. However, much more has to be improved, especially regarding the success of our cleaning procedure. Not only will this help us to reach the goal of transporting into the same lattice site with higher fidelity, but will also be useful in applications for other experiments as well. The aim was to first demonstrate that the experiments worked, and the next step is towards reproducibility and consistency.

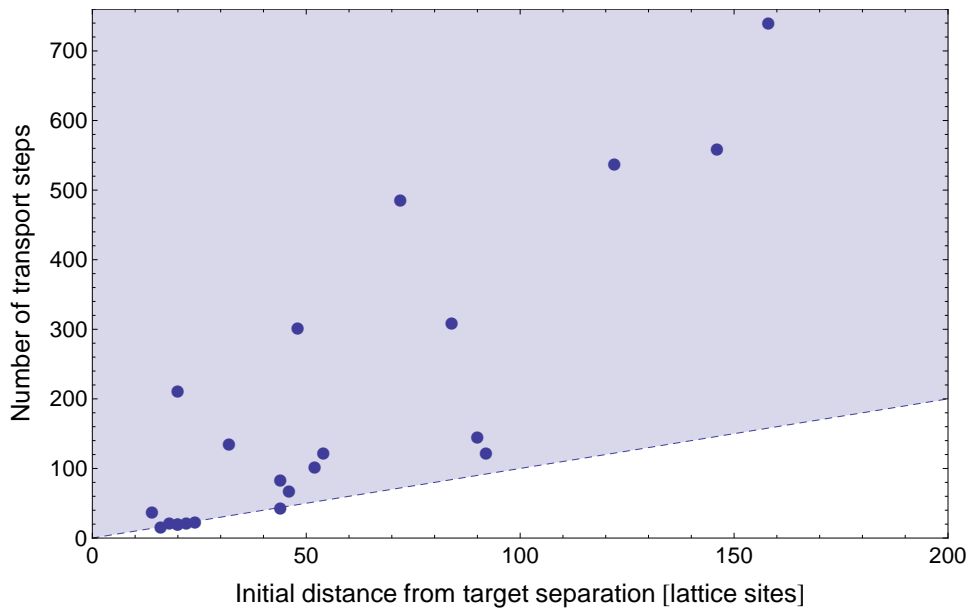


Figure 3.21: All successful sequences from Data 3: The data points represent all of the successful sequences that made it to the target separation of 10 lattice sites. Those sets that fall directly on the dotted-line of perfect transport took exactly the number of transport steps required for its initial atom separation.

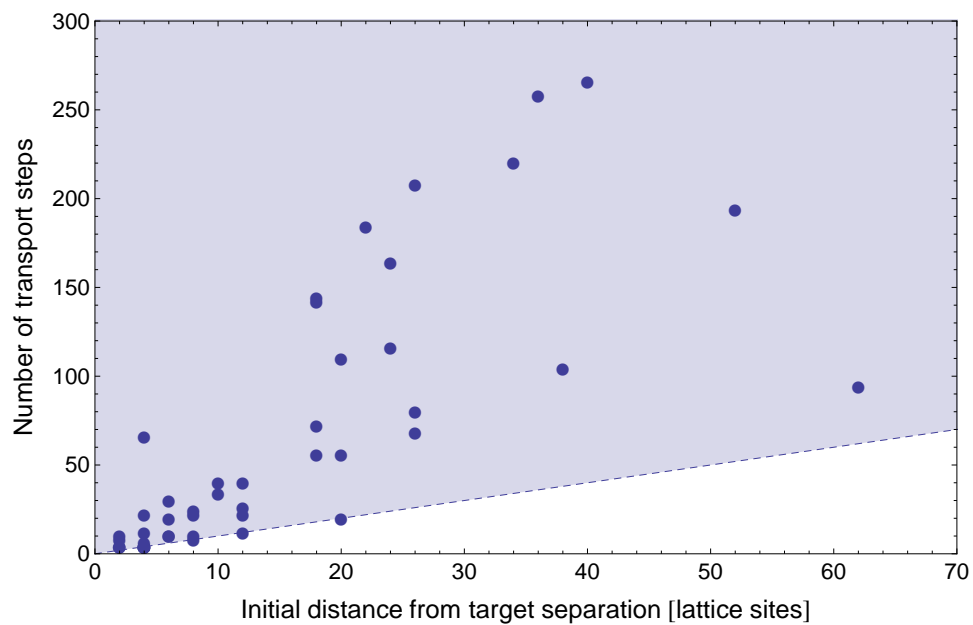


Figure 3.22: All successful sequences from Data 4: There are more data points than in Fig. 3.21 and thus more sequences that were successful in bringing the two atoms to a target separation of 4 lattice sites. This is because we have discarded less sequences that coincidentally had the two atoms already at or closer than the target separation. There are a few perfect sequences and many points which took far more transport steps.

# Chapter 4

## Conclusion

The principle of deterministic atom sorting of neutral Cs atoms trapped in a 1D optical lattice, has been demonstrated using our established state-dependent transport methods as well as incorporating new feedback methods. We have seen the results of two experiments, the first: transport of a single atom to an absolute target position along the lattice, and second: transport of two atoms, together, towards a target separation of as close as 4 lattice sites distance.

In the first set of experiments, we saw that  $> 60\%$  of all 120 newly-loaded atom sequences ended successfully with the atom at the target site. Most of those sequences took many more transport steps to reach the target than their initial distances required, which confirmed the need to have feedback for error corrections. There were also a few sequences which exhibited perfect transport and a few which jumped in the correct direction, causing the transport to occur in fewer steps. When we analyzed the individual reactions that took place per image in all of the sequences (not only those which were successful in the end), we observed and reported on the transport successes, transport errors, atom losses, and atom jumps. What was most interesting to find was that atom losses resulted in all atoms being lost and not just the target ones. Also, atoms jumped randomly across lattice sites and were more likely to occur for a set containing more atoms. Both behaviors are yet unexplainable, and will be tested further for a better understanding.

In the two atom experiments, we were able to bring two atoms together first to a separation of 10 lattice sites, and then 4. A reaction procedure involved the typical transport from the single atom measurements, as well as cleaning and atom addressing through the use of tunable, adiabatic passages applied to flip the state of an atom all while under a magnetic field gradient. Address and transport had a success rate of  $> 40\%$  where the non-successes were dominated by eventual atom losses. The cleaning procedure only worked perfectly for about 20% of the attempts, which is quite low. We will try to improve the algorithm as well as take some more tests regarding the performance of the adiabatic passages. Overall, we can say however, that the cleaning option improved atom sorting because we could initialize the system before transporting and it was easier to track the atoms independently between movements. And with fewer atoms to transport, there were less jumps observed.

The starting steps of classical atom sorting have been successfully demonstrated as we have seen in these proof of principle experiments. The next steps and ongoing work will involve optimizing the reaction procedures, especially cleaning, which has applications in the quantum walks experiments. Additionally, we will investigate the phenomena behind atom jumps to gain an understanding for our system. Eventually, we will also attempt to move atoms to the same lattice site for producing entanglement and also begin looking at quantum coherent transport.



## Chapter 5

### Next Steps and Prospects for Continuing Work

There is still much to be done in this topic and plans for continuing work for the next few months. This includes optimization of all of the reaction procedures, especially cleaning which has applications in other experiments such as quantum walks [4]. Just like in the single atom measurements, for quantum walks, we lose information when atoms are too close together and we try to transport them. Atoms are often loaded very close to one another due to being transferred from a densely packed MOT cloud. For this reason we cannot detect which atom has moved where. With a cleaning application, we can pick atoms that are spaced farther apart (at a minimum distance of 10 lattice sites) and would improve our measurement collection efficiency by almost threefold.

Another experiment to perform is to explore the behavior of atom jumps. This also has applications in quantum walks because the phenomenon is also seen there and is especially important to understand because the entire idea behind quantum walks is that the walks follow a characteristic probability distribution. Random jumping to different lattice sites skews this distribution. Proposals for experiments are to ramp the EOM back and forth and observe whether atoms jump or are lost between imaging. There would be no MW pulses applied and thus no transport. In principle, the atoms should remain in place but perhaps the EOM causes these jumps to occur. Another proposal is to simply take images one after another to see if the camera imaging could be a problem.

After improving procedures and getting a better understanding of the atom behavior, we also want to achieve the ultimate goal of transporting two atoms together into the same lattice site. This becomes challenging because we start to deal with atoms approaching each other from very small distances, or neighboring lattice sites.

In the distant future, there is also the possibility of performing quantum coherent transport which would occur on a much shorter timescale in the range of microseconds within the decoherence time of cesium. At the moment, this transport is purely classical and happens on a timescale of milliseconds. Coherent transport would exhibit more complicated but also interesting behavior due to the interference effects that rise from transporting superposition states.



# Bibliography

- [1] Seth Lloyd. Universal quantum simulators. *Science*, 273(5278):1073–1078, Aug. 23 1996.
- [2] M.A. Nielsen and I.L. Chuang. *Quantum Computation and Quantum Information*. Cambridge Series on Information and the Natural Sciences. Cambridge University Press, 2000.
- [3] Andreas Steffen, Andrea Alberti, Wolfgang Alt, Noomen Belmechri, Sebastian Hild, Michał Karski, Artur Widera, and Dieter Meschede. Digital atom interferometer with single particle control on a discretized space-time geometry. *Proceedings of the National Academy of Sciences*, 2012.
- [4] Michał Karski, Leonid Förster, Jai-Min Choi, Andreas Steffen, Wolfgang Alt, Dieter Meschede, and Artur Widera. Quantum walk in position space with single optically trapped atoms. *Science*, 325(5937):174–177, 2009.
- [5] Michał Karski, Leonid Förster, Jai-Min Choi, Andreas Steffen, Noomen Belmechri, Wolfgang Alt, Dieter Meschede, and Artur Widera. Imprinting patterns of neutral atoms in an optical lattice using magnetic resonance techniques. *New Journal of Physics*, 12(6):065027, 2010.
- [6] Andrea Alberti, Wolfgang Alt, Noomen Belmechri, Sebastian Hild, Michał Karski, Andreas Steffen, Artur Widera, and Dieter Meschede. Discrete interferometer with individual trapped atoms. In *QIAP Conference*, 2011.
- [7] Michał Karski. *State-selective transport of single neutral atoms*. PhD thesis, Rheinischen Friedrich-Wilhelms-Universität Bonn, 2010.
- [8] Microsoft. Named pipes- windows dev center, 2012. [Online; accessed 18-September-2012].
- [9] Wikipedia. Binomial distribution — wikipedia, the free encyclopedia, 2012. [Online; accessed 18-September-2012].
- [10] M. Khudaverdyan, W. Alt, I. Dotsenko, L. Förster, S. Kuhr, D. Meschede, Y. Miroshnychenko, D. Schrader, and A. Rauschenbeutel. Adiabatic quantum state manipulation of single trapped atoms. *Phys. Rev. A*, 71:031404, Mar 2005.
- [11] Mkrtych Khudaverdyan. Addressing of individual atoms in an optical dipole trap. Master’s thesis, Rheinischen Friedrich-Wilhelms-Universität, 2003.



# Acknowledgements

I would like to thank my advisor Prof. Dieter Meschede, as well as Bonn International Graduate School (BIGS) for guiding me during my two years of Masters studies and funding my stay here in Bonn. For giving me the opportunity to not only do compelling physics research, but to explore and learn a different culture to my own, I am undoubtedly grateful. I would also like thank Prof. Stefan Linden for being the co-grader of my thesis along with my advisor.

The research group of Prof. Meschede, especially Andrea Alberti and Andreas Steffen, have given good advice and fostered new ideas together with me. Andreas has been in the laboratory for all of the measurements and his extensive knowledge and experience have been useful, not to mention his patience and persistence. Noomen Belmechri, Wolfgang Alt, and Kotya Karapetyan have also given me valuable insight during my final month of my Masters thesis.

Finally, I thank my friends and family who have helped me keep my motivation, and my boyfriend Fabian who has also given me good advice and help.



# Declaration

I hereby certify that the work presented here was accomplished by myself and without the use of illegitimate means or support, and that no sources and tools were used other than those cited.

Bonn, \_\_\_\_\_

Date

Signature